NASA TECHNICAL MEMORANDUM

NASA TM X-3475


NASA TM X-3475



# AERODYNAMIC CHARACTERISTICS AT MACH 6 OF A HYPERSONIC RESEARCH AIRPLANE CONCEPT HAVING A 70° SWEPT DELTA WING

*Louis E. Clark and Christine B. Richie*

*Langley Research Center*
*Hampton, Va. 23665*

NATIONAL AERONAUTICS AND SPACE ADMINISTRATION • WASHINGTON, D. C. • MAY 1977

| 1. Report No. | 2. Government Accession No. | 3. Recipient's Catalog No. |
|---|---|---|
| NASA TM X-3475 | | |

| 4. Title and Subtitle | 5. Report Date |
|---|---|
| AERODYNAMIC CHARACTERISTICS AT MACH 6 OF A HYPERSONIC RESEARCH AIRPLANE CONCEPT HAVING A 70° SWEPT DELTA WING | May 1977 |
| | 6. Performing Organization Code |

| 7. Author(s) | 8. Performing Organization Report No. |
|---|---|
| Louis E. Clark and Christine B. Richie | L-10712 |
| | 10. Work Unit No. 505-11-31-02 |
| 9. Performing Organization Name and Address<br>NASA Langley Research Center<br>Hampton, VA 23665 | 11. Contract or Grant No. |
| | 13. Type of Report and Period Covered<br>Technical Memorandum |
| 12. Sponsoring Agency Name and Address<br>National Aeronautics and Space Administration<br>Washington, DC 20546 | 14. Sponsoring Agency Code |

15. Supplementary Notes

16. Abstract

An experimental investigation was conducted at Mach 6 to determine the hypersonic aerodynamic characteristics of an air-launched, delta-wing research aircraft concept. Included was the effect of various components such as nose shape, wing camber, wing location, center vertical tail, wing tip fins, forward delta wing, engine nacelle, and speed brakes. Tests were conducted with a 0.021-scale model at a Reynolds number, based on model length, of $10.5 \times 10^6$ and over an angle-of-attack range from $-4^\circ$ to $20^\circ$.

The experimental results show that most configurations with a center vertical tail have static longitudinal stability at trim, static directional stability at angles of attack up to $12^\circ$, and static lateral stability throughout the angle-of-attack range. Configurations with wing tip fins generally have static longitudinal stability at trim, have lateral stability at angles of attack above $8^\circ$, and are directionally unstable over the angle-of-attack range.

| 17. Key Words (Suggested by Author(s)) | 18. Distribution Statement |
|---|---|
| Hypersonic aircraft<br>Hypersonic stability and control<br>Lift<br>Aerodynamics | Unclassified - Unlimited<br><br>Subject Category 02 |

| 19. Security Classif. (of this report) | 20. Security Classif. (of this page) | 21. No. of Pages | 22. Price* |
|---|---|---|---|
| Unclassified | Unclassified | 58 | $4.50 |

* For sale by the National Technical Information Service, Springfield, Virginia 22161

# AERODYNAMIC CHARACTERISTICS AT MACH 6 OF A HYPERSONIC RESEARCH AIRPLANE CONCEPT HAVING A 70° SWEPT DELTA WING

Louis E. Clark and Christine B. Richie
Langley Research Center

## SUMMARY

An experimental investigation was conducted at Mach 6 to determine the hypersonic aerodynamic characteristics of an air-launched, delta-wing research aircraft concept. Included was the effect of various components such as nose shape, wing camber, wing location, center vertical tail, wing tip fins, forward delta wing, engine nacelle, and speed brakes. Tests were conducted with a 0.021-scale model at a Reynolds number, based on model length, of $10.5 \times 10^6$ and over an angle-of-attack range from $-4^\circ$ to $20^\circ$.

The experimental results show that most configurations with a center vertical tail have static longitudinal stability at trim, static directional stability at angles of attack up to $12^\circ$, and static lateral stability throughout the angle-of-attack range. Configurations with wing tip fins generally have static longitudinal stability at trim, have lateral stability at angles of attack above $8^\circ$, and are directionally unstable over the angle-of-attack range.

## INTRODUCTION

Hypersonic aircraft of the future are expected to be liquid-hydrogen fueled and scramjet powered. A high-speed, air-launched research airplane has been proposed in reference 1 to determine the aerodynamic potential of these integrated engine/airframe aircraft and to demonstrate the use of hydrogen-fueled scramjets, actively cooled airframes, cryogenic tanks, and other advanced technology.

Air-launched research-aircraft concepts have been developed since they are much smaller, more economical, and less complex than concepts designed for ground take-off. These air-launched concepts are constrained in size and weight by the capabilities and geometry of the launch aircraft. The concept considered in the present study would be air launched from a C-5A at a Mach number of 0.8 and rocket accelerated to a Mach number of 8 or 10 for a scramjet cruise mission. The fuselage, which is 10.7 meters long, was sized to accommodate the rocket propellant and hydrogen fuel required for this mission. The delta wing has a $70^\circ$ leading-edge sweep and a maximum span of 10.7 meters.

Additional studies have shown that a concept having lower maximum Mach number and air launched from a B-52 is a more feasible system when initial and total costs of the research program are carefully analyzed (refs. 2 and 3).

The purpose of the present investigation was to determine the effect of various components on the aerodynamic characteristics of the C-5A launched research-

aircraft concept at a Mach number of 6. The variations tested included alternate forebodies, forward delta wing, center vertical tail, wing tip fins, engine nacelle, wing camber, wing location, and speed brakes. Experimental studies of this concept at subsonic and supersonic speeds have been reported in references 4 and 5.

## SYMBOLS

The longitudinal characteristics are presented about the stability axes, and the lateral-directional characteristics are presented about the body axes. The body-axis and stability-axis systems are illustrated in figure 1. The moment reference point was at the design center-of-gravity location which was at a longitudinal station 64.5 percent of the fuselage length and a vertical station 1.3 percent of the fuselage length below the vehicle reference line. Values are given in SI Units and, where useful, also in U.S. Customary Units. Measurements and calculations were made in U.S. Customary Units.

$A_r$ reference area, area of 70° delta wing including fuselage intercept

$b$ wing span

$C_D$ drag coefficient, $D/q_\infty A_r$

$C_L$ lift coefficient, $L/q_\infty A_r$

$C_{L_\alpha}$ rate of change of $C_L$ with angle of attack per degree

$C_l$ rolling-moment coefficient, $M_X/q_\infty A_r b$

$C_{l_\beta}$ rate of change of $C_l$ with angle of sideslip per degree

$C_m$ pitching-moment coefficient, $M_Y/q_\infty A_r \ell$

$C_{m_\alpha}$ rate of change of $C_m$ with angle of attack per degree

$\partial C_m/\partial C_L$ rate of change of $C_m$ with lift coefficient (longitudinal stability parameter)

$C_n$ yawing-moment coefficient, $M_Z/q_\infty A_r b$

$C_{n_\beta}$ rate of change of $C_n$ with angle of sideslip per degree

$C_Y$ side-force coefficient, $F_Y/q_\infty A_r$

$C_{Y_\beta}$ rate of change of $C_Y$ with angle of sideslip per degree

$D$ drag, $F_N \sin \alpha + F_A \cos \alpha$

$F_A$ axial force along X-axis; positive direction, -X

$F_N$ normal force along Z-axis; positive direction, -Z

$F_Y$ side force along Y-axis; positive direction, +Y

L lift, $F_N \cos \alpha - F_A \sin \alpha$

L/D lift-drag ratio

$\ell$ length of model fuselage

$M_X, M_Y, M_Z$ moments about X-, Y-, and Z-axes, respectively

$q_\infty$ free-stream dynamic pressure

X,Y,Z reference axes

$\alpha$ angle of attack, degrees

$\beta$ angle of sideslip, degrees

$\delta$ elevon-deflection angle, positive when trailing edge is down, degrees

Subscripts:

s stability-axis system

t trim condition, $C_m = 0$

Model component designations:

$B_1$ high profile nose

$B_2$ low profile nose

E scramjet engine

$F_D$ forward delta wing

$S_B$ speed brakes

$V_c$ center vertical tail

$V_t$ wing tip fins

$W_1$ positively cambered wing

$W_2$ negatively cambered wing

The subscripts f and a are used with the model component designations to indicate forward location and aft location.

## APPARATUS AND TEST PROCEDURE

The tests were conducted in the Langley 20-inch Mach 6 tunnel. This is a blowdown-type wind tunnel with a two-dimensional nozzle and a square test section 50.8 centimeters (20 inches) wide. This facility is discussed in more detail in reference 6.

Tests were conducted at a nominal stagnation pressure of 2.72 MPa and a nominal stagnation temperature of 483 K. These conditions correspond to a nominal free-stream Reynolds number, based on model length, of $10.5 \times 10^6$. The angle of attack was varied from $-4^\circ$ to $20^\circ$ for sideslip angles of $0^\circ$ and $-4^\circ$, and the elevon settings were varied from $10^\circ$ to $-20^\circ$.

Forces and moments were measured with an internally mounted six-component strain-gage balance. The model was mounted on a movable support and driven through several angles of attack or sideslip during each run. Angles of attack and sideslip were set by using a prism mounted on the model to reflect light from a source onto a calibrated chart. Mach number was obtained at each test point with a pitot-pressure probe in the test section, located to avoid interference with the model.

The model base pressure was determined from the average of two measurements, and the axial force was adjusted to correspond to a base pressure equal to free-stream static pressure. Straight-line slopes between data at $0^\circ$ and $-4^\circ$ sideslip were used to obtain the lateral-directional stability parameters.

The estimated probable uncertainties in the force and moment coefficients were obtained by using the superposition of errors theorem from reference 7. The accuracy-of-balance calibration, zero shift of balance during tests, computer readout, dynamic pressure, and pressure transducers were considered in estimating the probable uncertainties. These uncertainties are estimated to be within the following limits:

| | |
|---|---|
| $C_L$ | $\pm 0.0036$ |
| $C_D$ | $\pm 0.0012$ |
| L/D | $\pm 0.12$ |
| $C_m$ | $\pm 0.0004$ |
| $C_{l_\beta}$ | $\pm 0.0001$ |
| $C_{n_\beta}$ | $\pm 0.00009$ |
| $C_{Y_\beta}$ | $\pm 0.0009$ |

The accuracy of angle of attack and sideslip is estimated to be $\pm 0.10^\circ$, and the accuracy of free-stream Mach number is estimated to be $\pm 0.02$.

## MODEL

A 0.021-scale stainless-steel model of the delta-wing, hypersonic research aircraft used in the present tests is shown in figures 2 and 3. The model was constructed so that various components could be installed on a basic fuselage, as shown in figures 4 and 5. These components consisted of two nose shapes, a

forward delta wing, positively and negatively cambered wings, wing-tip fins, a center vertical tail, 20° speed brakes, and a flow-through scramjet engine. The nose shapes represented two alternate cockpit locations. The forward delta wing was employed to minimize the shift of the aerodynamic center with Mach number. A negatively cambered wing was used to assess the effect of camber in trimming the aircraft. A center vertical tail and wing tip fins were employed to determine their comparative effectiveness in providing directional stability. The wing was capable of being mounted at two longitudinal locations. The model base was modified from the scalloped design (ref. 4) of the full-scale aircraft to a semicircular shape to allow installation of the force balance. Elevons were adjustable in 5° increments from 10° to -20°. Table I gives geometric details of the model.

## RESULTS AND DISCUSSION

### Static Longitudinal Characteristics

Configuration buildup.- The results of a configuration buildup with body $B_1$ are shown in figure 6. The incomplete configuration $B_1W_{1f}$ is generally stable over the angle-of-attack range and has the highest maximum lift-drag ratio of the $B_1$ configurations tested. Addition of wing tip fins ($B_1W_{1f}V_t$) increased the drag and stability, caused a slight increase in lift with angle of attack, and reduced the maximum lift-drag ratio. The slight increase in lift with angle of attack which occurred with the wing tip fins ($B_1W_{1f}V_t$) could be due to a reduction in pressure bleedoff around the wing tips and suggests the use of small tip fins with zero toe-in on the wing bottom surface to obtain additional L/D. Addition of the forward delta wing ($B_1W_{1f}V_tF_D$) increased the lift forward of the center of gravity with a resultant decrease in stability. Addition of the scramjet engine nacelle ($B_1W_{1f}V_tF_DE$) increased both lift and drag, decreased the lift-drag ratio, and slightly reduced the longitudinal stability. The complex flow pattern about the scramjet is shown in figure 3, and the exact cause of the increased lift is difficult to isolate. Results obtained for a limited number of components with body $B_2$ show similar trends (fig. 7).

Effect of components.- A comparison of data for bodies $B_1$ and $B_2$ shows, as expected, that the body with the more slender nose ($B_2$) is slightly less unstable, causing a reduction in the trim angle of attack from 10.5° for the $B_1W_{1f}V_t$ configuration to 7° for the $B_2W_{1f}V_t$ configuration (figs. 6 and 7).

Tests with the positively cambered wing mounted in the aft location, when compared with the forward data, showed an increase in stability with only small changes in other characteristics (fig. 8). Although the negatively cambered wing ($B_1W_{2f}V_t$) increased the positive pitching moment, the configuration was unstable for $\alpha$ greater than 6° with a decrease in L/D (fig. 9).

Use of the center vertical tail ($B_1W_{1f}V_c$) resulted in decreased drag, lift, and stability but increased maximum L/D (fig. 10), as compared with the $B_1W_{1f}V_t$ configuration. The addition of 20° speed brakes to the center vertical tail caused large increases in stability and drag but decreases in maximum L/D and lift at low angles of attack. The effectiveness of the speed brakes

decreased with angle of attack; at high angles of attack the aerodynamic characteristics were approaching the values for the undeflected center vertical tail.

Effect of elevon deflections on trim characteristics.- The longitudinal characteristics were obtained at elevon deflections from 10° to -20° for five configurations: $B_1W_{1f}V_t$, $B_1W_{1f}V_tE$, $B_1W_{1f}V_tF_D$, $B_1W_{1f}V_tF_DE$, and $B_1W_{1f}V_c$, shown in figures 11, 12, 13, 14, and 15, respectively. Characteristics for a reduced range of elevon deflections were obtained for configurations $B_1W_{1a}V_c$ and $B_1W_{2f}V_t$ and are shown in figures 16 and 17. Longitudinal trim characteristics were obtained both from the data and from cross plots for elevon deflections between experimental points (figs. 18 and 19).

Most configurations were stable at trim near the maximum lift-drag ratio. The maximum values of L/D at trim occurred at angles of attack between 8° and 10.5° and ranged from 3.25 for the $B_1W_{1f}V_c$ configuration to 2.80 for the $B_1W_{1f}V_tE$ configuration. Configurations with the forward delta wing or positively cambered wing with concentrations of lift forward of the center of gravity required positive elevon deflections for trim over the angle-of-attack range; whereas single-delta-wing configurations required both positive and negative elevon deflections for trim. Reduction in L/D due to trim was about 0.15 for most configurations. Generally, the configurations showed a tendency for pitchup at the higher negative elevon deflections with increasing angle of attack.

Effect of sideslip.- The minor effect of sideslip angle (from 0° to -4°) on the longitudinal characteristics shown in figure 20 for the $B_1W_{1f}V_t$ configuration is typical, with the exception of the speed-brake configuration (fig. 21) which experienced a decrease in drag and pitching moment and small changes in L/D and $C_L$ with sideslip.

## Static Lateral-Directional Characteristics

Configuration buildup.- The results of a configuration buildup with body $B_1$ are shown in figure 22. Body $B_1$ has a small degree of lateral stability and is directionally unstable. Addition of the delta wing ($B_1W_{1f}$) had essentially no effect on the directional stability but did produce a large change in the lateral stability which varied from destabilizing to stabilizing as the angle of attack increased. The wing tip fins ($B_1W_{1f}V_t$) substantially decreased the directional instability and had essentially no effect on the lateral stability. Addition of the forward delta wing ($B_1W_{1f}V_tF_D$) had essentially no effect on either the lateral or directional stability. The flow-through scramjet engine did not affect the lateral-directional characteristics. Results obtained for a limited number of components with body $B_2$ show similar trends (fig. 23).

Effect of components.- A comparison of the data for bodies $B_1$ and $B_2$ (figs. 22 and 23) shows that, as expected, a slight decrease in directional instability was exhibited by body $B_2$ with the slender nose. Tests with the positively cambered wing mounted in the aft location showed a decrease in directional instability with only small changes in other characteristics (fig. 24).

The effectiveness of wing tip fins, as compared with the effectiveness of a center vertical tail, is shown in figure 25. The configuration with wing tip fins was directionally unstable over the angle-of-attack range but possessed lateral stability at angles of attack above approximately $8^{\circ}$. The configuration with the center vertical tail was directionally stable at angles of attack up to about $8^{\circ}$ and was laterally stable over the angle-of-attack range. The addition of $20^{\circ}$ speed brakes to the center vertical tail produced large increases in both directional and lateral stability at the lower angles of attack. The effectiveness of the speed brakes decreased with angle of attack; and at $\alpha = 16^{\circ}$, the lateral-directional characteristics approached the values for the undeflected center vertical tail.

Installation of the forward delta wing on the configuration with a center vertical tail resulted in a positive increment in directional stability with angle of attack, which did not occur when the forward delta wing was added to the configuration with wing tip fins (fig. 26). This may be due to an interaction of the center vertical tail with the vortex flow which occurs on the lee surface. The lateral stability was improved by the addition of the forward delta wing.

The negatively cambered wing when combined with either the center-vertical-tail configuration or the wing-tip configuration provided a favorable increment in lateral stability which decreased with increasing angle of attack (fig. 27). The directional stability of the center-vertical-tail configuration was unaffected by the use of the negatively cambered wing; whereas the wing-tip-fin configuration showed a change in directional stability which varied from stabilizing to destabilizing with increasing angle of attack.

## SUMMARY OF RESULTS

An experimental investigation has been conducted at a Mach number of 6 and a Reynolds number, based on model length, of $10.5 \times 10^6$ to determine the hypersonic aerodynamic characteristics of a delta-wing research aircraft concept in which a number of different designs of fuselage, wing, and vertical tail were included. An analysis of the experimental data has led to the following summary of results:

1. Most of the model configurations were stable at trim. Single-delta-wing configurations trimmed at both positive and negative elevon deflections whereas configurations employing the forward delta wing required positive elevon deflections for trim.

2. Addition of the forward delta wing increased the lift and decreased the longitudinal stability.

3. Addition of a flow-through scramjet engine increased lift and drag, substantially decreased the maximum lift-drag ratio, and slightly decreased the longitudinal stability. Essentially no change in either lateral or directional stability was noted with the addition of the scramjet engine.

4. Although the model configuration with the negatively cambered wing had increased positive pitching moment, the configuration was unstable for angles of attack greater than $6^{\circ}$ and had a decreased maximum lift-drag ratio.

5. Model configurations with wing tip fins, as compared with configurations with a center vertical tail, had increased drag, lift, and longitudinal stability but a smaller maximum lift-drag ratio.

6. Addition of $20^{\circ}$ speed brakes to the center vertical tail resulted in a large increase in drag and longitudinal, directional, and lateral stability but a large decrease in lift and lift-drag ratio at low angles of attack. The effectiveness of the speed brakes decreased with angle of attack, and at high angles of attack the aerodynamic characteristics approached the values for the undeflected center vertical tail.

7. At lower angles of attack the center vertical tail was much more effective in providing directional stability than were the wing tip fins. The effectiveness of the center vertical tail decreased with angle of attack while the effectiveness of wing tip fins remained about constant. Consequently, at the highest angle of attack, tip fins became more effective.

8. Model configurations with tip fins were directionally unstable over the angle-of-attack range whereas the configurations with a center vertical tail were stable at angles of attack up to about $8^{\circ}$.

9. The center vertical tail provided a substantial increment in lateral stability, and configurations with this tail were stable throughout the angle-of-attack range. Wing tip fins reduced lateral stability, and configurations with these fins were stable at angles of attack greater than about $8^{\circ}$.

10. Addition of the forward delta wing to configurations with a center vertical tail resulted in a positive increment in directional stability with angle of attack, which did not occur when the forward delta wing was added to the configurations with wing tip fins.

11. Configurations with a center vertical tail possessed about the same directional stability with either the positively or negatively cambered wing, but on models with wing tip fins the negatively cambered wing produced an increment which ranged from stabilizing to destabilizing with increasing angle of attack.

12. The negatively cambered wing provided a favorable increment in lateral stability over the positively cambered wing for both vertical-fin configurations.

Langley Research Center
National Aeronautics and Space Administration
Hampton, VA 23665
January 20, 1977

## REFERENCES


1. Nagel, A. L.; and Becker, J. V.: Key Technology for Airbreathing Hypersonic Aircraft. AIAA Paper No. 73-58, Jan. 1973.

2. Kirkham, Frank S.; Jackson, L. Robert; and Weidner, John P.: The Case for a High-Speed Research Airplane - Results From an In-House Study. AIAA Paper No. 74-988, Aug. 1974.

3. Kirkham, F. S.; Jones, R. A.; Buck, M. L.; and Zima, W. P.: Joint USAF/NASA Hypersonic Research Aircraft Study. AIAA Paper No. 75-1039, Aug. 1975.

4. Creel, Theodore R., Jr.; and Penland, Jim A.: Low Speed Aerodynamic Characteristics of a Hypersonic Research Airplane Concept Having a 70° Swept Delta Wing. NASA TM X-71974, 1974.

5. Penland, Jim A.; Fournier, Roger H.; and Marcum, Don C., Jr.: Aerodynamic Characteristics of a Hypersonic Research Airplane Concept Having a 70° Swept Double-Delta Wing at Mach Numbers From 1.50 to 2.86. NASA TN D-8065, 1975.

6. Goldberg, Theodore J.; and Hefner, Jerry N. (appendix by James C. Emery): Starting Phenomena for Hypersonic Inlets With Thick Turbulent Boundary Layers at Mach 6. NASA TN D-6208, 1971.

7. Leaver, R. H.; and Thomas, T. R.: Analysis and Presentation of Experimental Results. John Wiley & Sons, Inc., c.1974.

TABLE I.- GEOMETRIC CHARACTERISTICS OF MODEL

| | | |
|---|---|---|
| **Wing:** | | |
| Area, reference (includes fuselage intercept), $m^2$ ($in^2$) | 0.043 | (67.200) |
| Area, exposed, $m^2$ ($in^2$) | 0.023 | (36.121) |
| Area, wetted, $m^2$ ($in^2$) | 0.047 | (72.242) |
| Span, m (in.) | 0.217 | (8.542) |
| Aspect ratio | | 1.086 |
| Root chord, at fuselage center line, m (in.) | 0.353 | (13.896) |
| Tip chord, m (in.) | 0.085 | (3.355) |
| Taper ratio | | 0.241 |
| Mean aerodynamic chord, m (in.) | 0.248 | (9.779) |
| Sweepback angles: | | |
| Leading edge, deg | | 70 |
| 25-percent-chord line, deg | | 64 |
| Trailing edge, deg | | 0 |
| Dihedral angle, at airfoil mean line, deg | | -3.64 |
| Incidence angle, deg | | 0 |
| Airfoil section | | (See fig. 5(a)) |
| Airfoil thickness ratio: | | |
| Exposed root | | 0.05 |
| Tip | | 0.06 |
| Leading-edge radius at - | | |
| Fuselage-line chord, m (in.) | $5.08 \times 10^{-4}$ | (0.020) |
| Tip, m (in.) | $5.08 \times 10^{-4}$ | (0.020) |
| Area of both elevons, $m^2$ ($in^2$) | 0.005 | (7.161) |
| **Forward delta wing:** | | |
| Area exposed, outside of fuselage, forward of wing leading edge, $m^2$ ($in^2$) | 0.002 | (3.394) |
| Leading-edge sweep, deg | | 80 |
| **Tip fin:** | | |
| Area, each, $m^2$ ($in^2$) | 0.004 | (5.848) |
| Span, m (in.) | 0.069 | (2.730) |
| Aspect ratio | | 1.274 |
| Root chord, m (in.) | 0.086 | (3.383) |
| Tip chord, m (in.) | 0.029 | (1.135) |
| Taper ratio | | 0.336 |
| Mean aerodynamic chord, m (in.) | 0.062 | (2.445) |

TABLE I.- Concluded

| | | |
|---|---|---|
| Sweepback angles: | | |
| Leading edge, top, deg | | 55.0 |
| Leading edge, bottom, deg | | 70.1 |
| Trailing edge, top, deg | | 21.3 |
| Toe-in angle, deg | | 7.5 |
| Airfoil section: | | |
| Leading-edge radius, m (in.) | $5.08 \times 10^{-4}$ | (0.020) |
| **Center vertical tail:** | | |
| Area, exposed, $m^2$ ($in^2$) | 0.007 | (11.492) |
| Span, exposed, m (in.) | 0.086 | (3.380) |
| Aspect ratio of exposed area | | 0.994 |
| Root chord, at fuselage surface line, m (in.) | 0.128 | (5.040) |
| Tip chord, m (in.) | 0.045 | (1.760) |
| Taper ratio | | 0.349 |
| Mean aerodynamic chord of exposed area, m (in.) | 0.093 | (3.664) |
| Sweepback angles: | | |
| Leading edge, deg | | 55.0 |
| Trailing edge, deg | | 24.6 |
| Airfoil section: | | |
| Thickness ratio at - | | |
| Tip | | 0.106 |
| Root | | 0.106 |
| Leading-edge radius, m (in.) | $5.08 \times 10^{-4}$ | (0.020) |
| **Fuselage:** | | |
| Length, m (in.) | 0.508 | (20.000) |
| Maximum height, m (in.) | 0.071 | (2.782) |
| Maximum width, m (in.) | 0.073 | (2.866) |
| Fineness ratio of equivalent round body | | 6.822 |
| Planform area, $m^2$ ($in^2$) | 0.026 | (40.445) |
| Wetted area, $m^2$ ($in^2$) | 0.083 | (128.460) |
| Wetted area, with wing on, $m^2$ ($in^2$) | 0.078 | (120.695) |
| Wetted area, with both delta wings on, $m^2$ ($in^2$) | 0.077 | (118.747) |
| Base area, $m^2$ ($in^2$) | 0.002 | (3.726) |
| **Complete model, with both delta wings:** | | |
| Planform area, $m^2$ ($in^2$) | 0.052 | (79.960) |
| Aspect ratio of planform | | 0.913 |

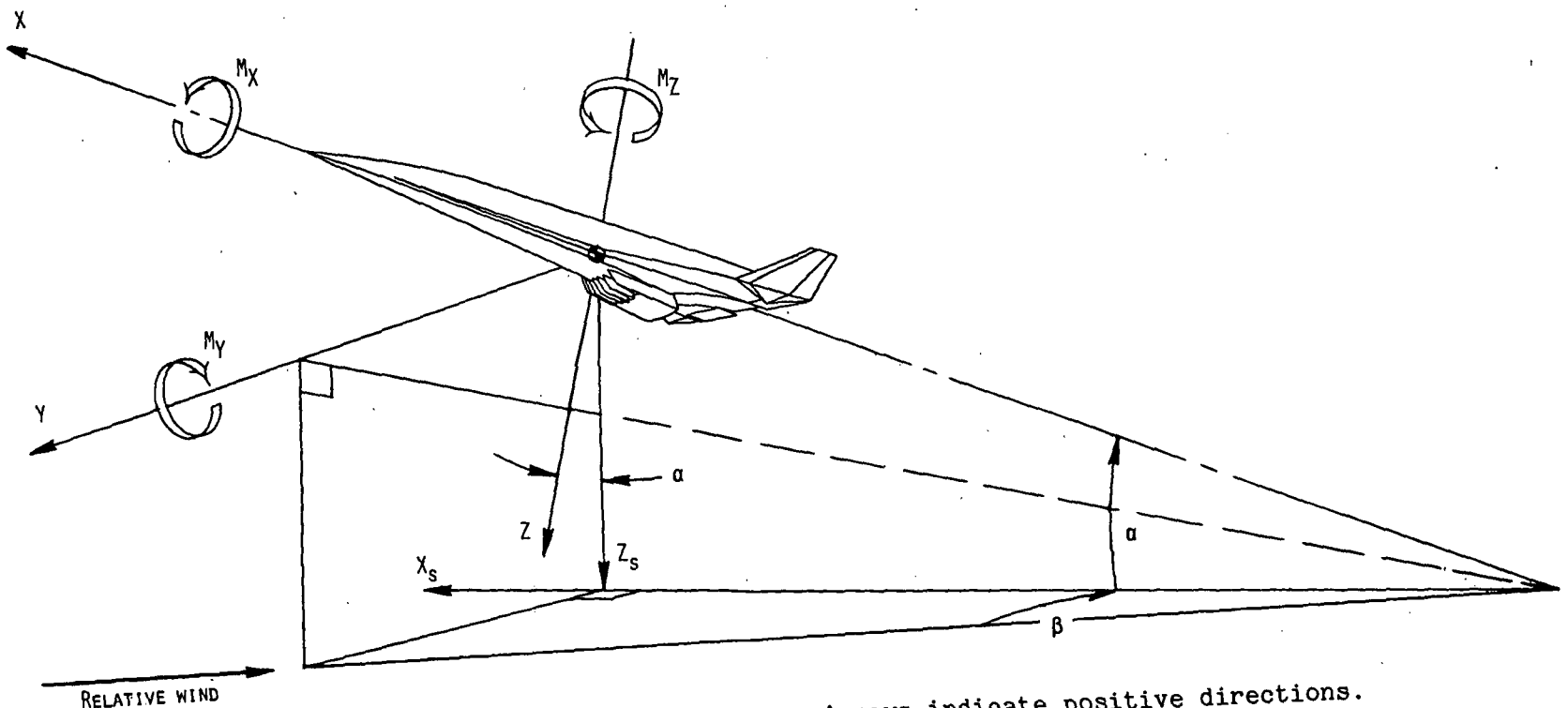


Figure 1.- Systems of reference axes. Arrows indicate positive directions.

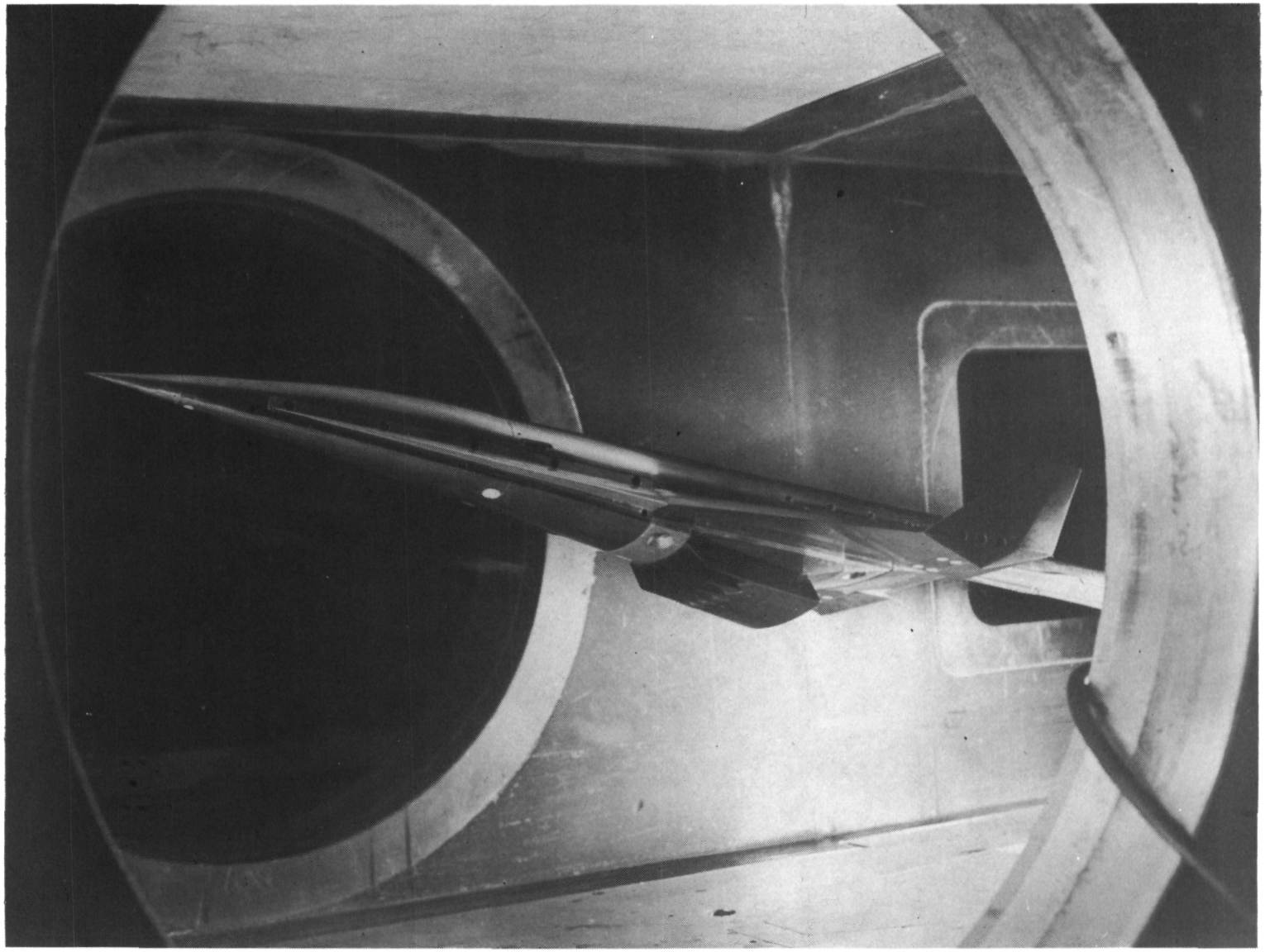

L-74-1669

Figure 2.- Model (configuration $B_1W_{1f}V_tF_DE$) installed in wind tunnel.

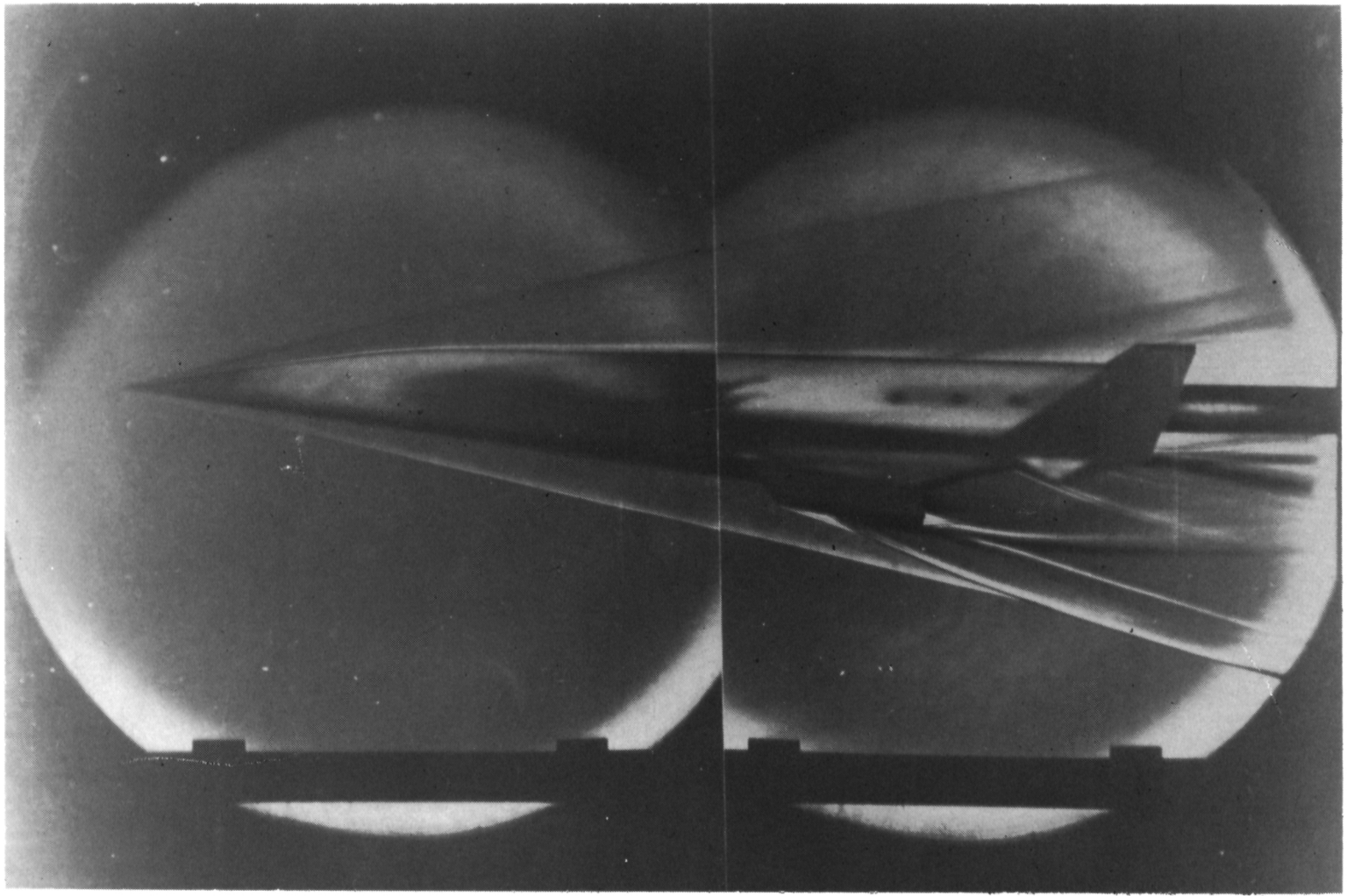

L-74-1930

(a) $\alpha = 0^{\circ}$.

Figure 3.- Composite schlieren photograph of model.

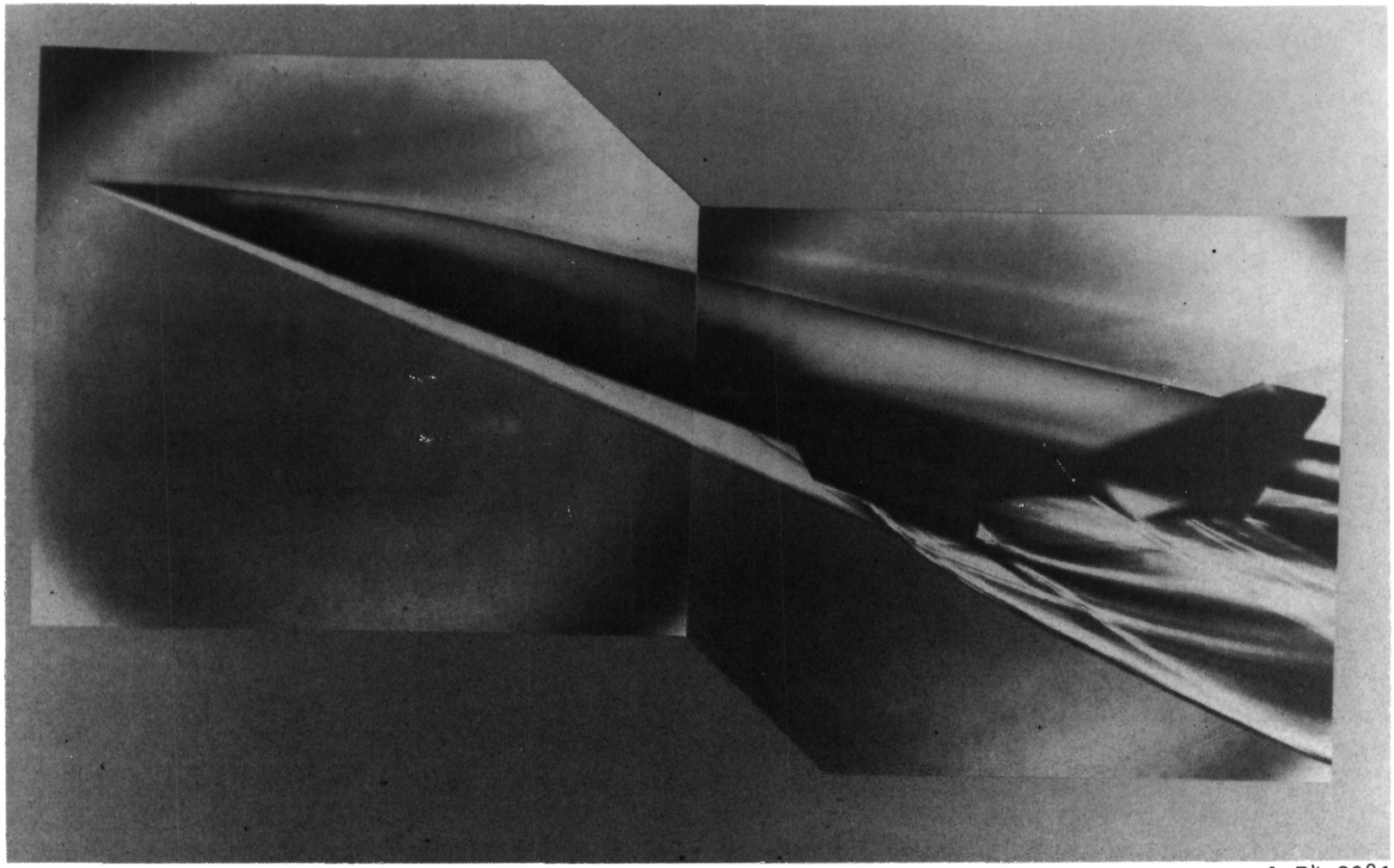

L-74-2081

(b) $\alpha = 10^{\circ}$.

Figure 3.- Concluded.

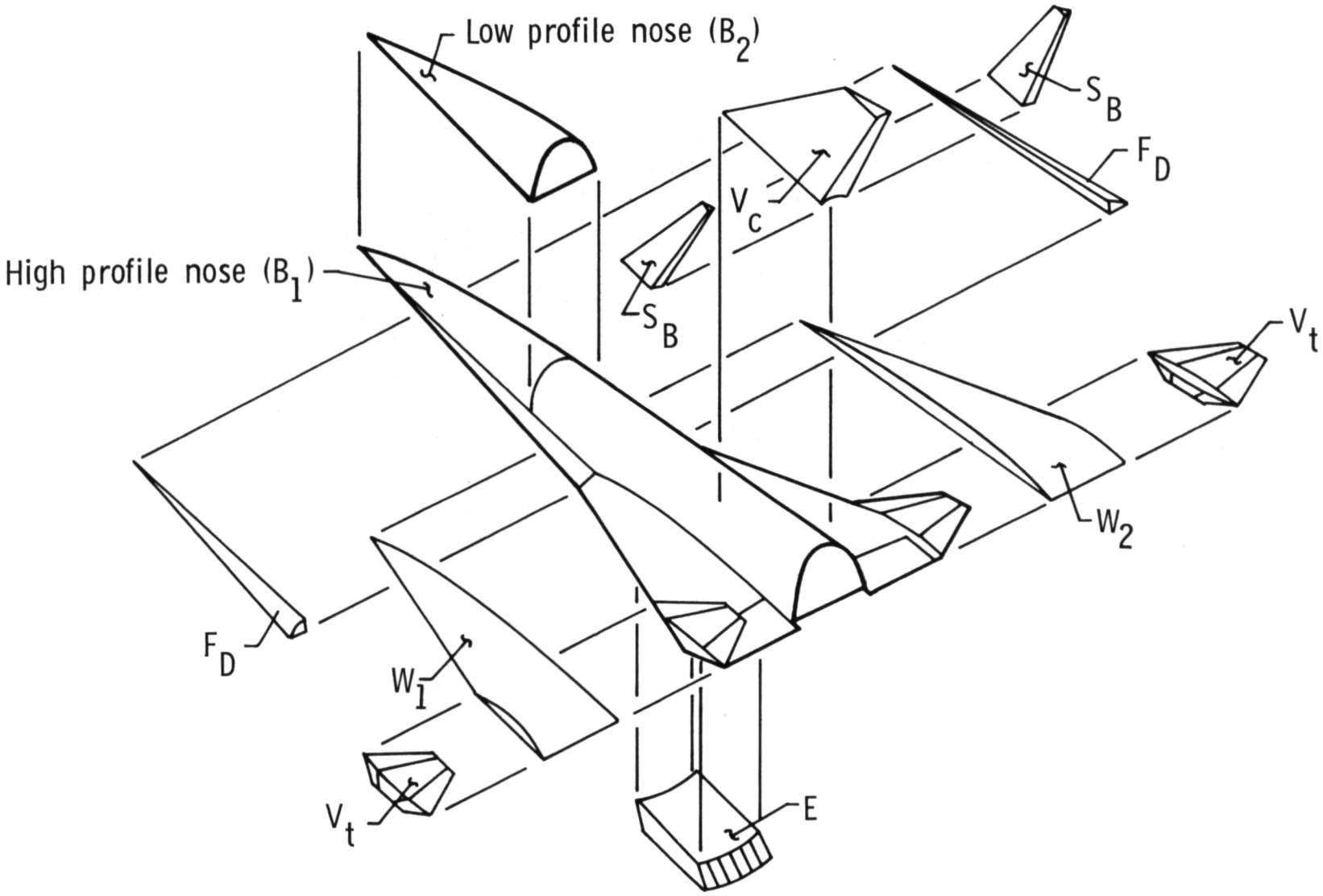


Figure 4.- Sketch of model used, showing interchangeable parts.

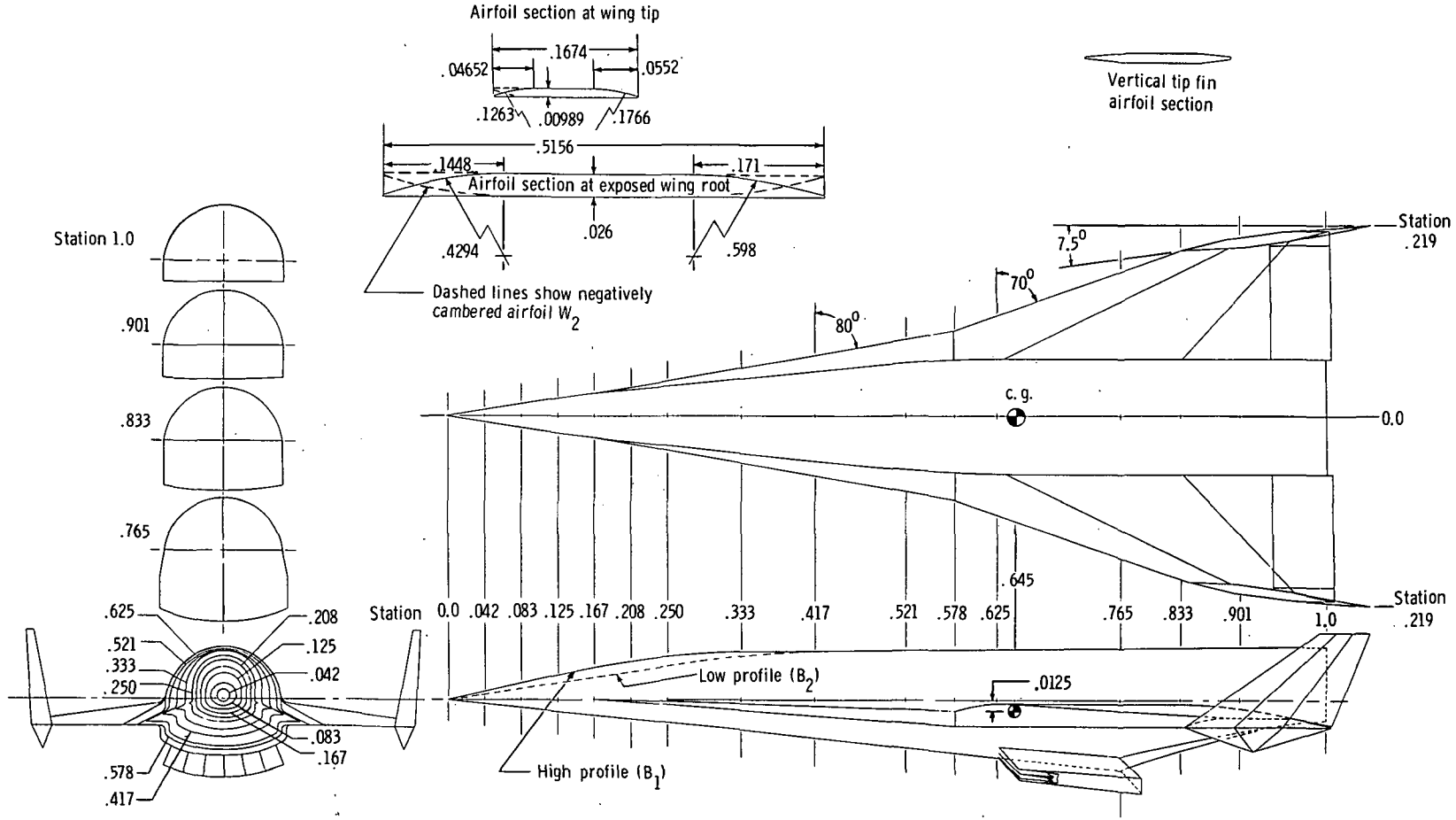


(a) Baseline configuration.

Figure 5.- Model general dimensions. All dimensions have been normalized by the body length ( $\ell$ = 50.8 cm).

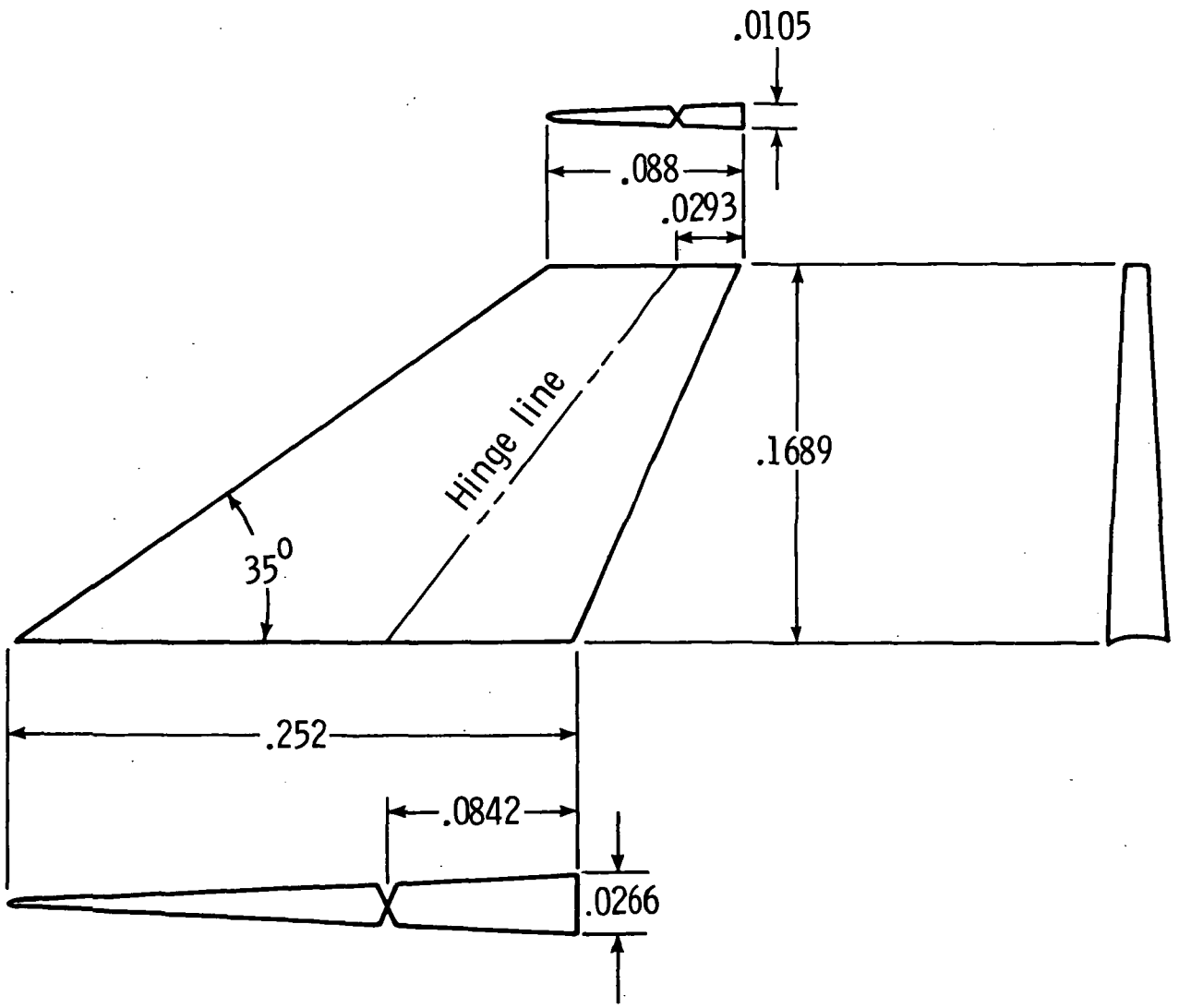


(b) Center vertical tail.

Figure 5.- Continued.

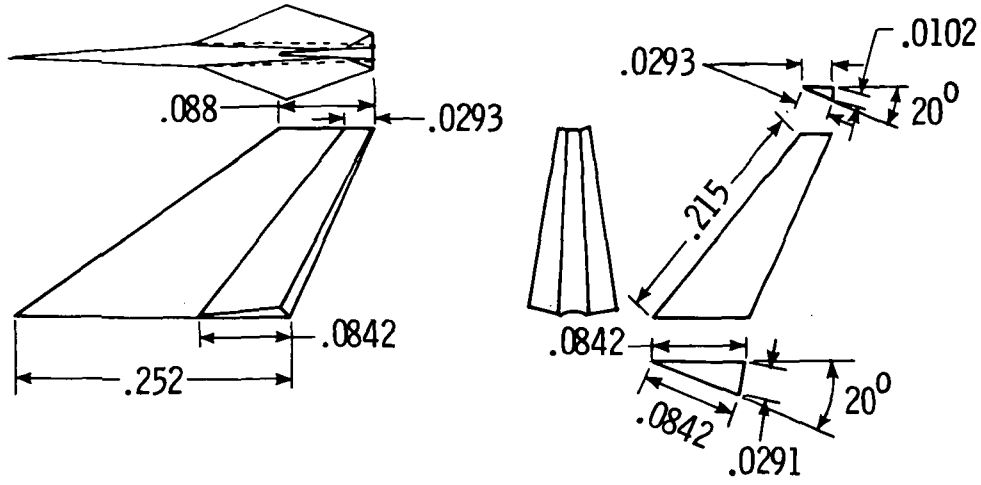


(c) Speed brakes.

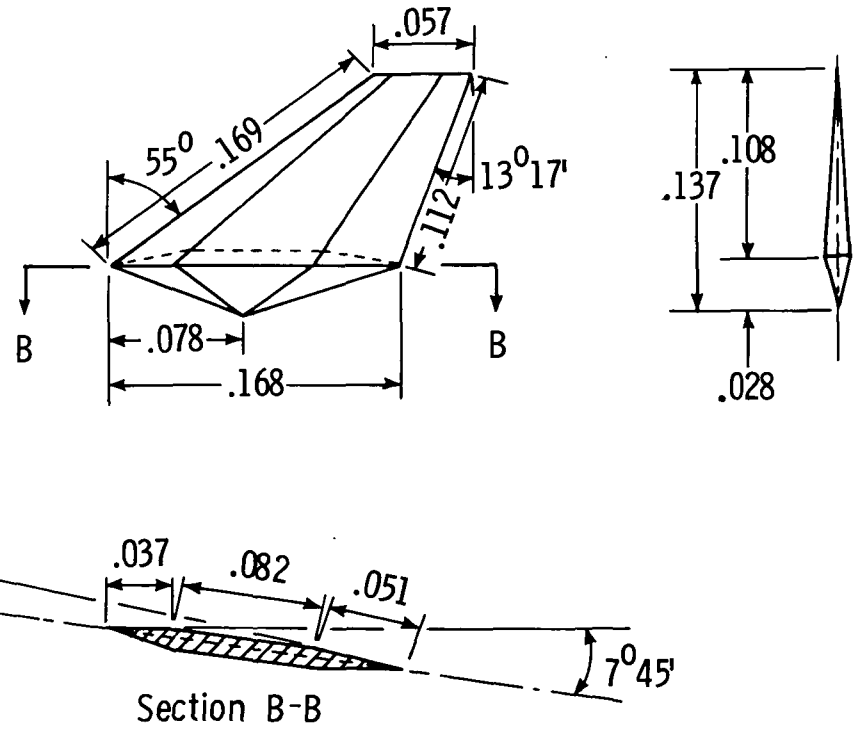


(d) Wing tip fins.

Figure 5.- Continued.

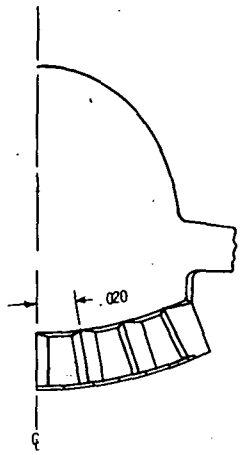


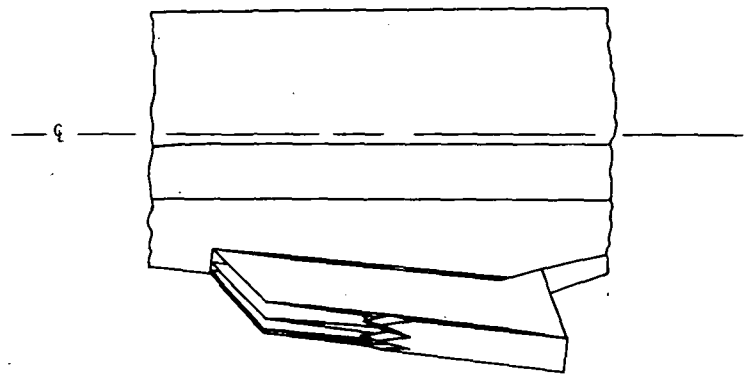


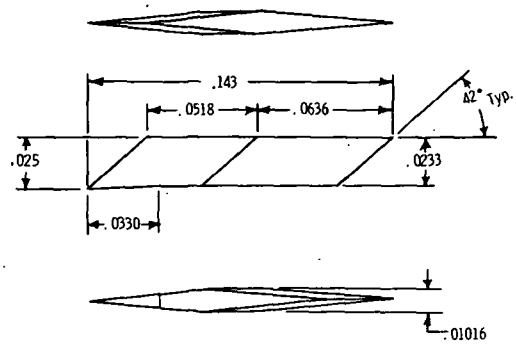


Inside splitter plate

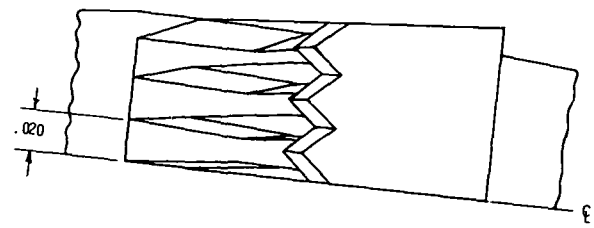


Bottom view of scramjet engine with cowl on

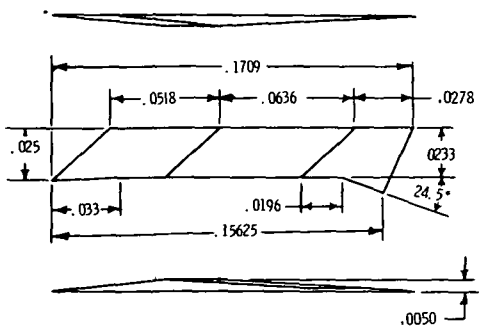


Left outside plate

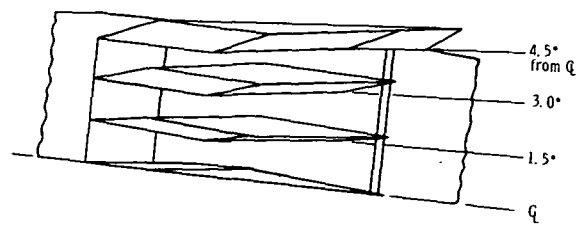


Bottom view of scramjet engine with cowl removed

(e) Scramjet engine.

Figure 5.- Concluded.

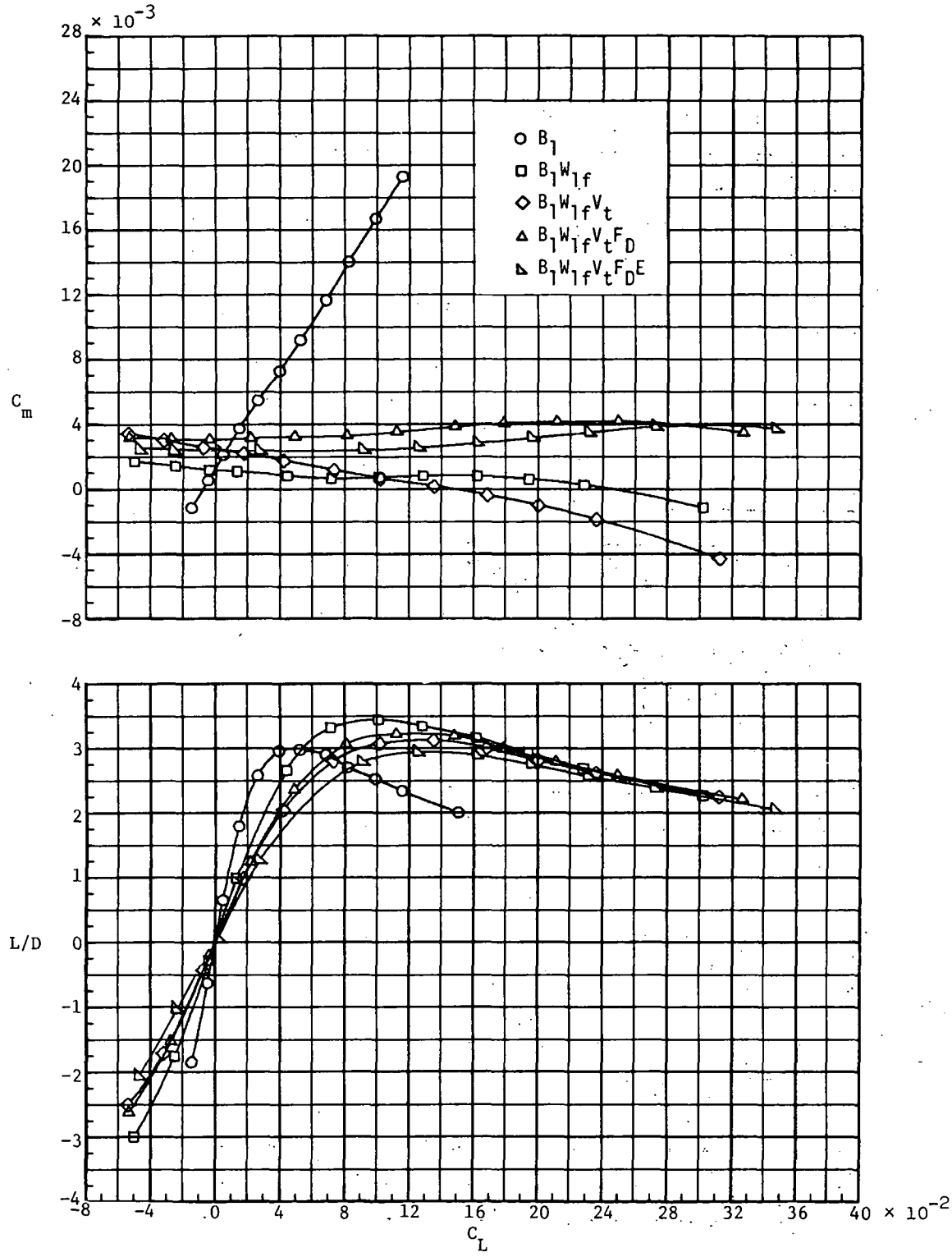


(a) Pitch and lift-drag ratio.

Figure 6.- Effect of configuration buildup on longitudinal characteristics with body $B_1$; $\delta = 0^\circ$.

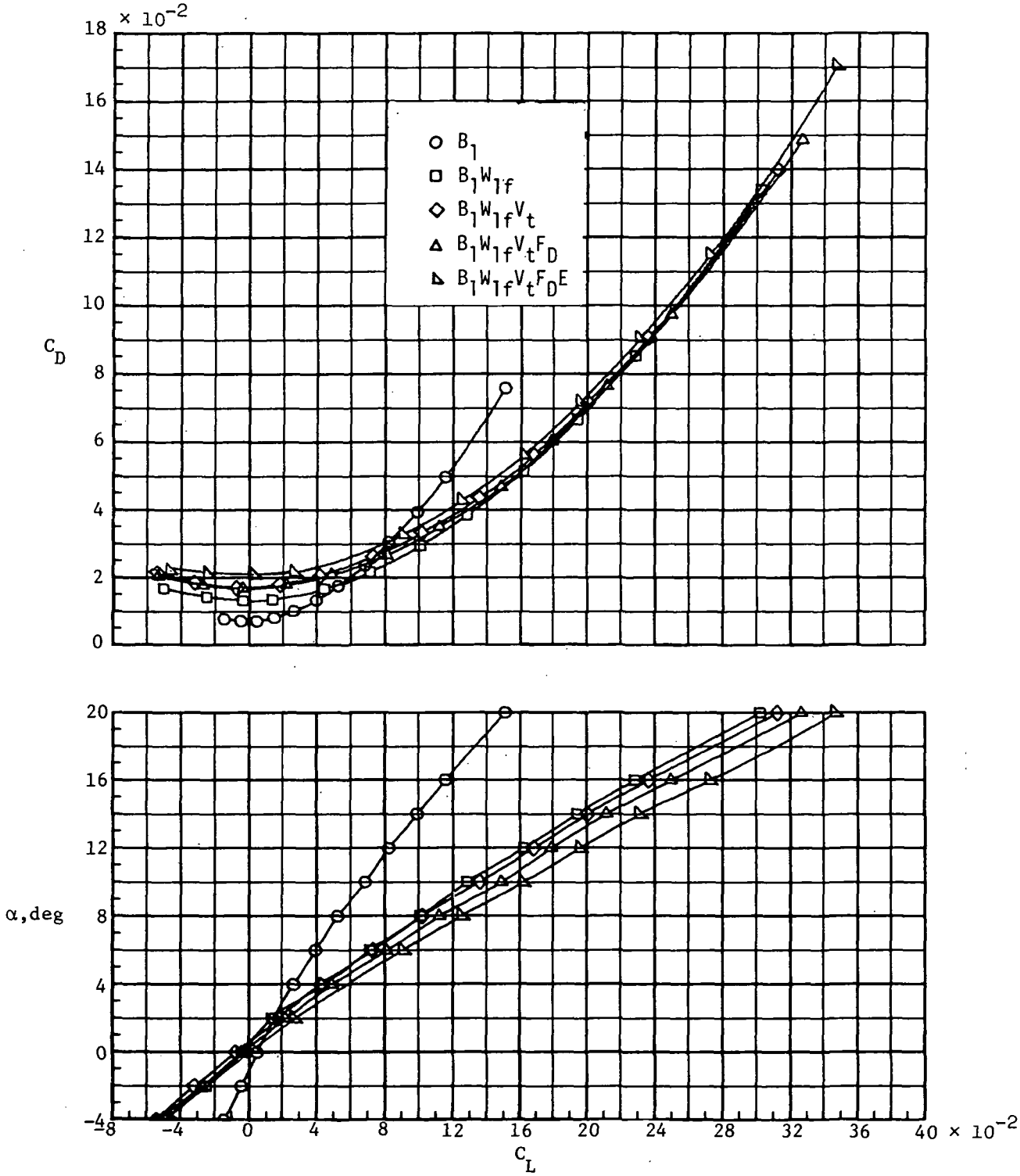


(b) Lift and drag.

Figure 6.- Concluded.

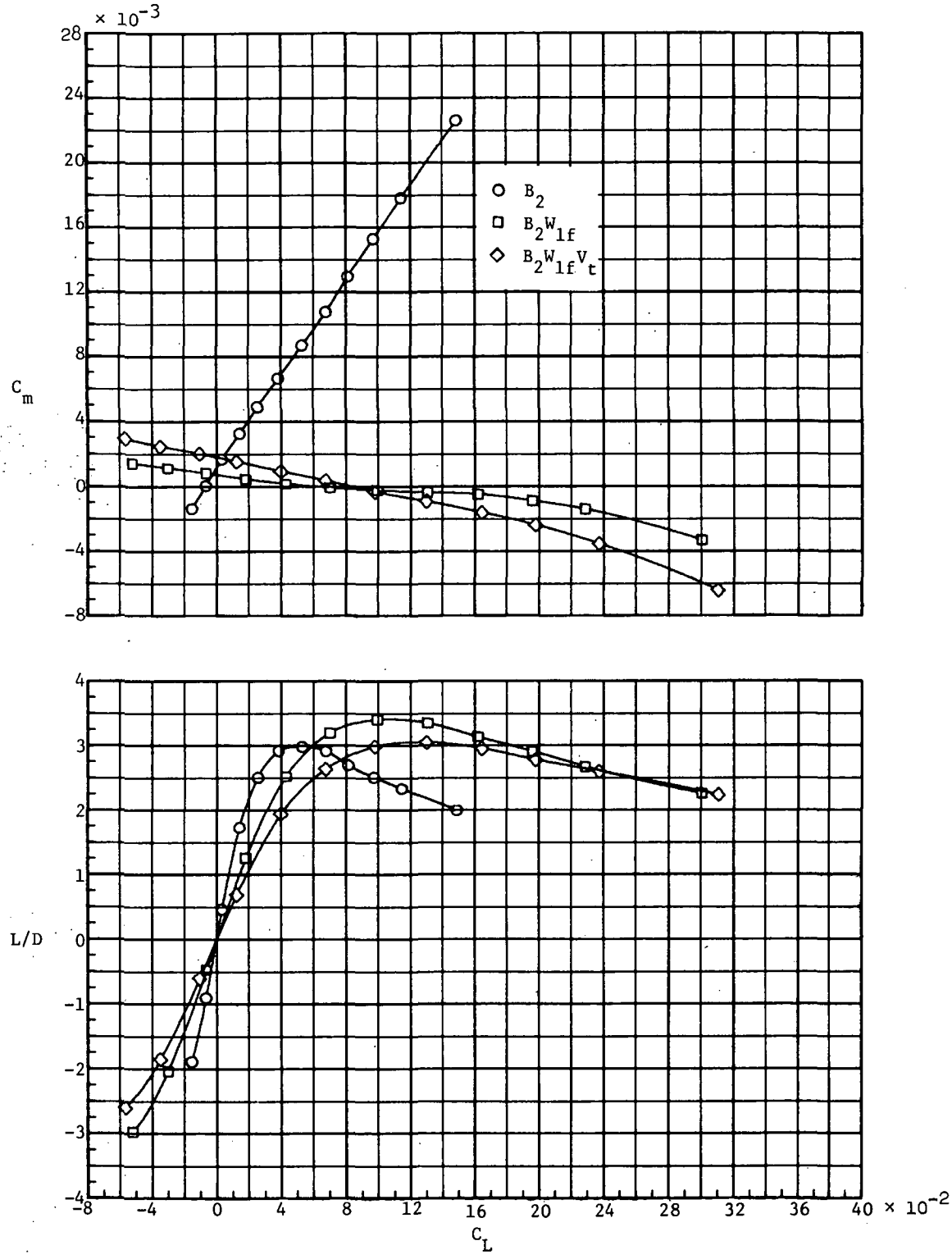


(a) Pitch and lift-drag ratio.

Figure 7.- Effect of components on longitudinal characteristics with body $B_2$; $\delta = 0^{\circ}$.

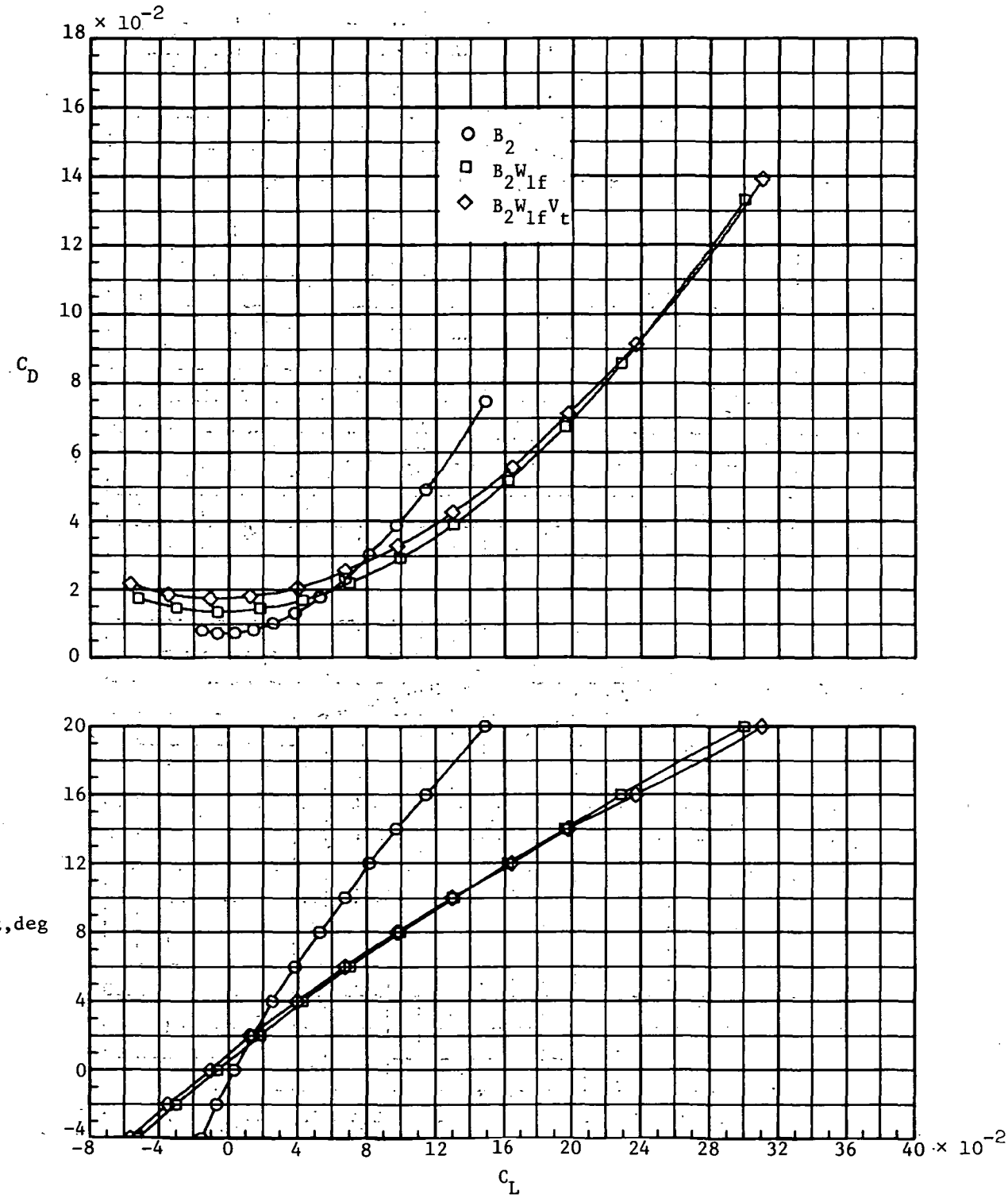


(b) Lift and drag.

Figure 7.- Concluded.

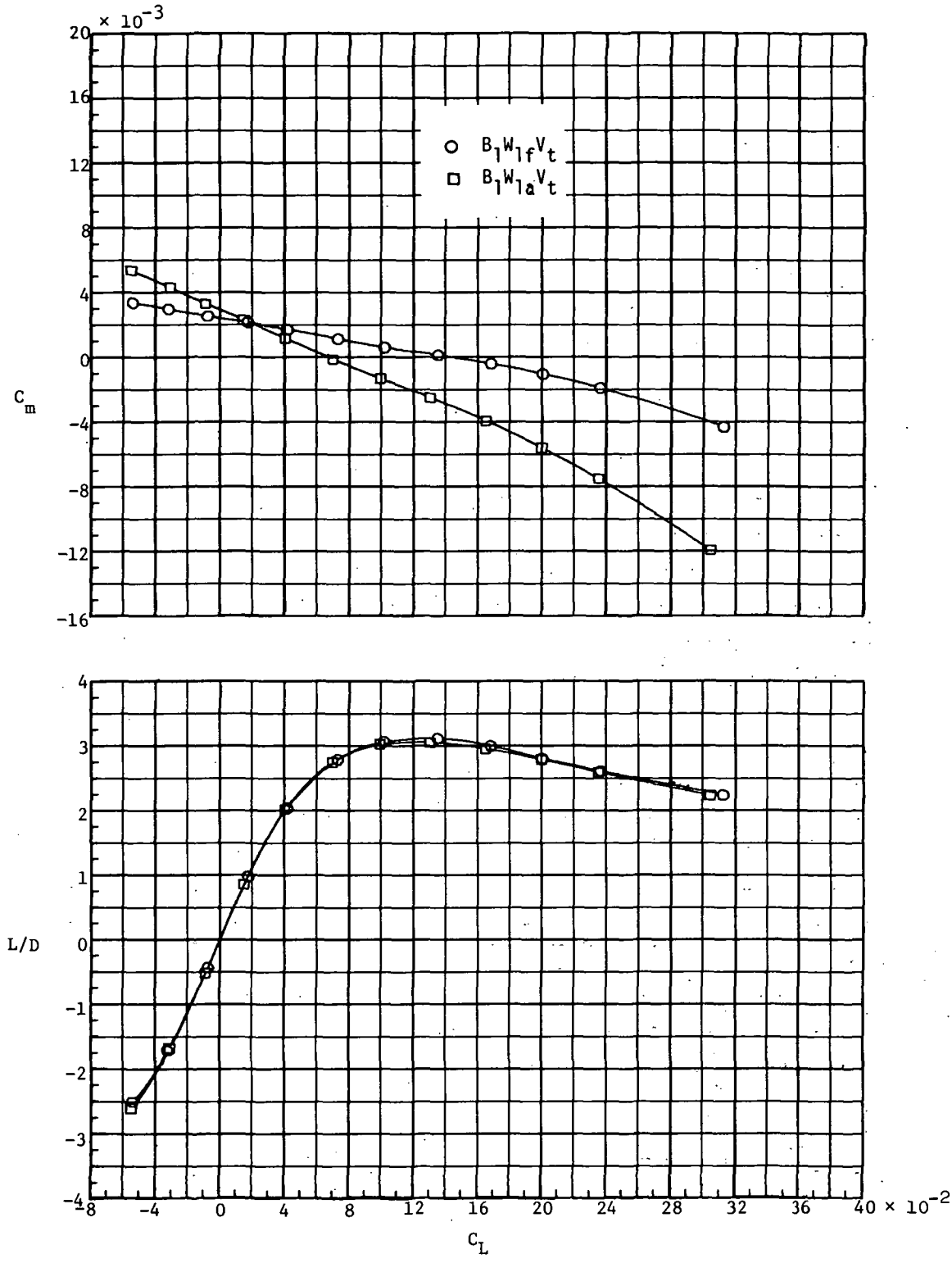


(a) Pitch and lift-drag ratio.

Figure 8.- Effect of wing location on longitudinal characteristics.

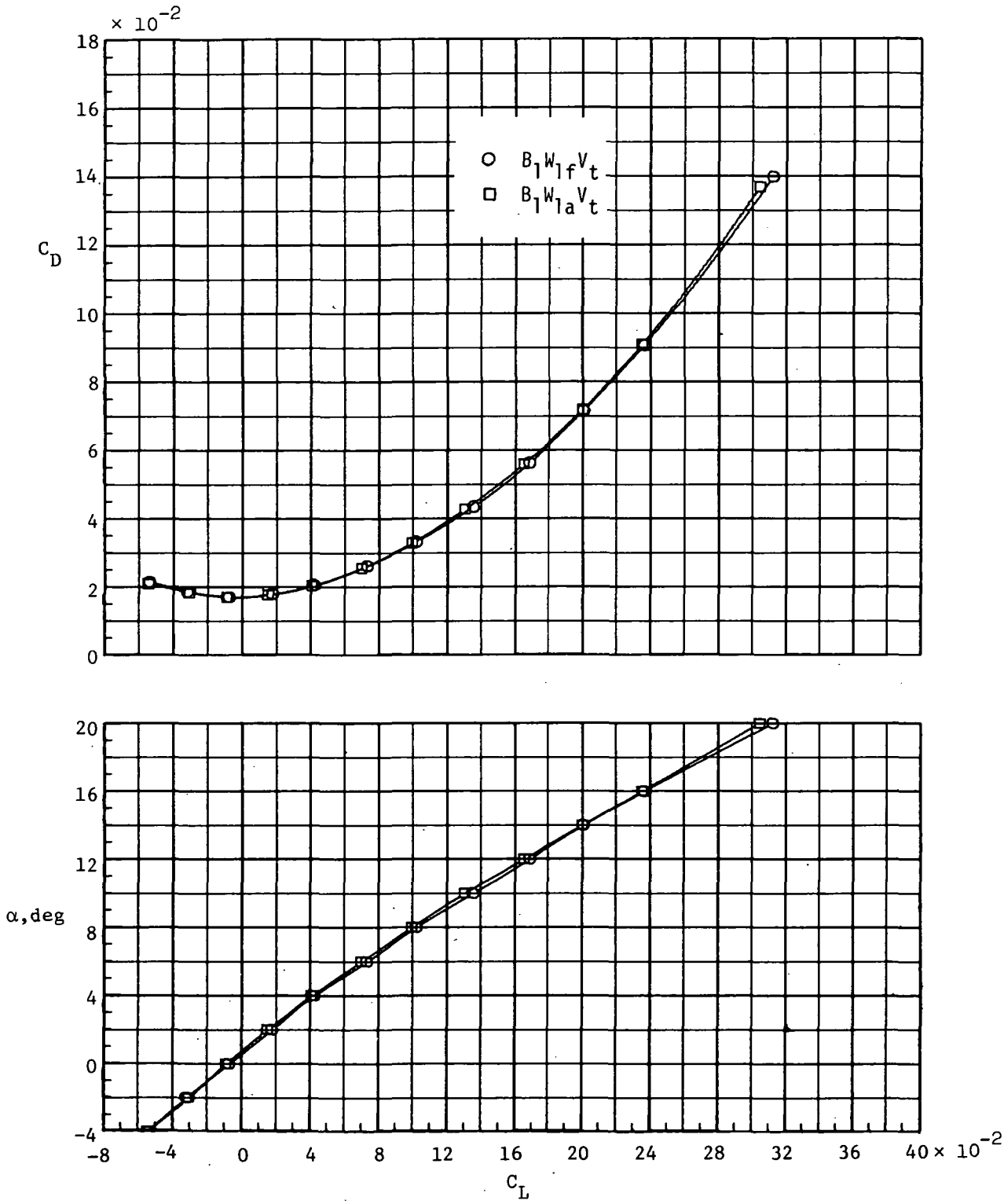


(b) Lift and drag.

Figure 8.- Concluded.

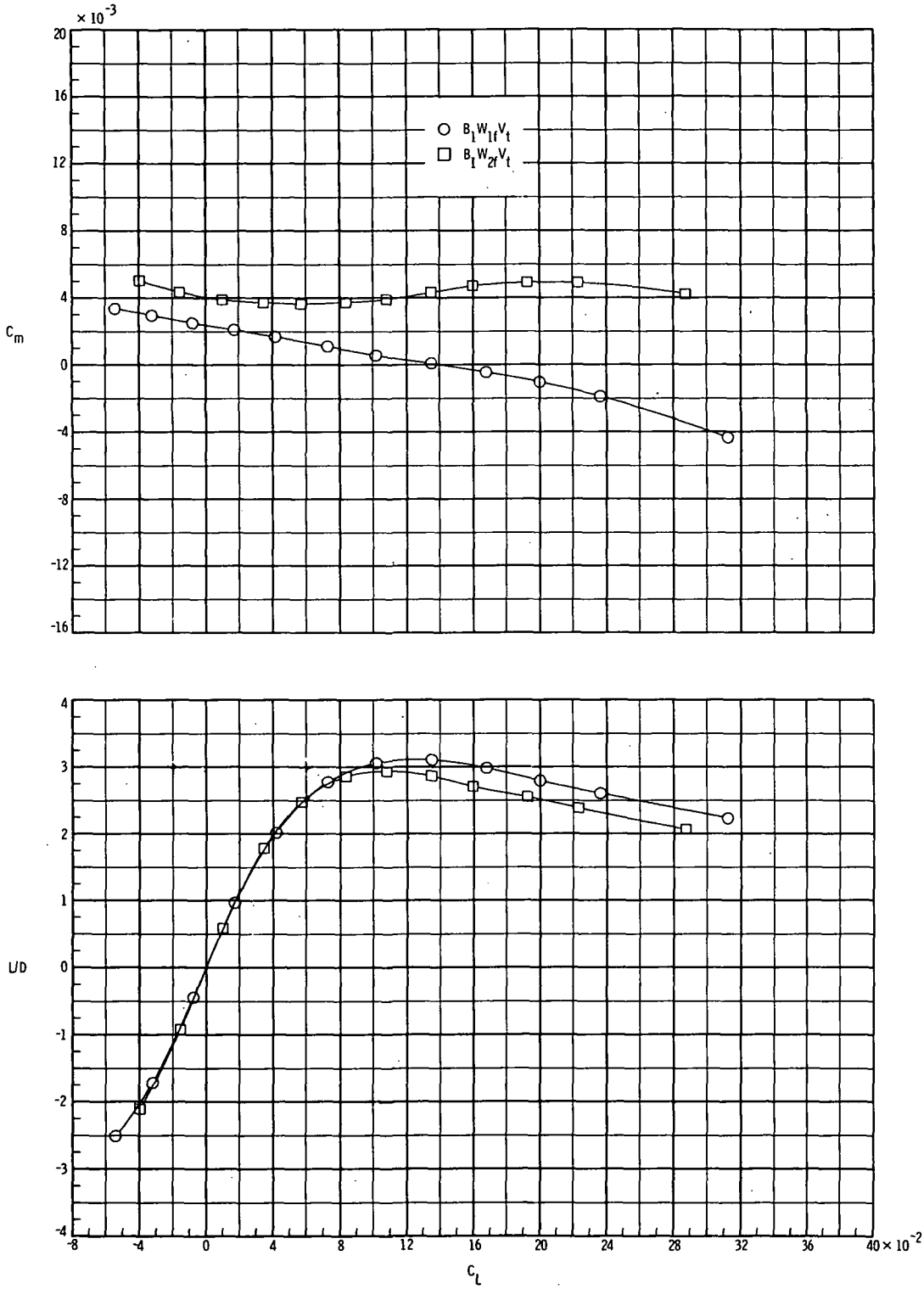


(a) Pitch and lift-drag ratio.

Figure 9.- Effect of wing camber on longitudinal characteristics; $\delta = 0^{o}$.

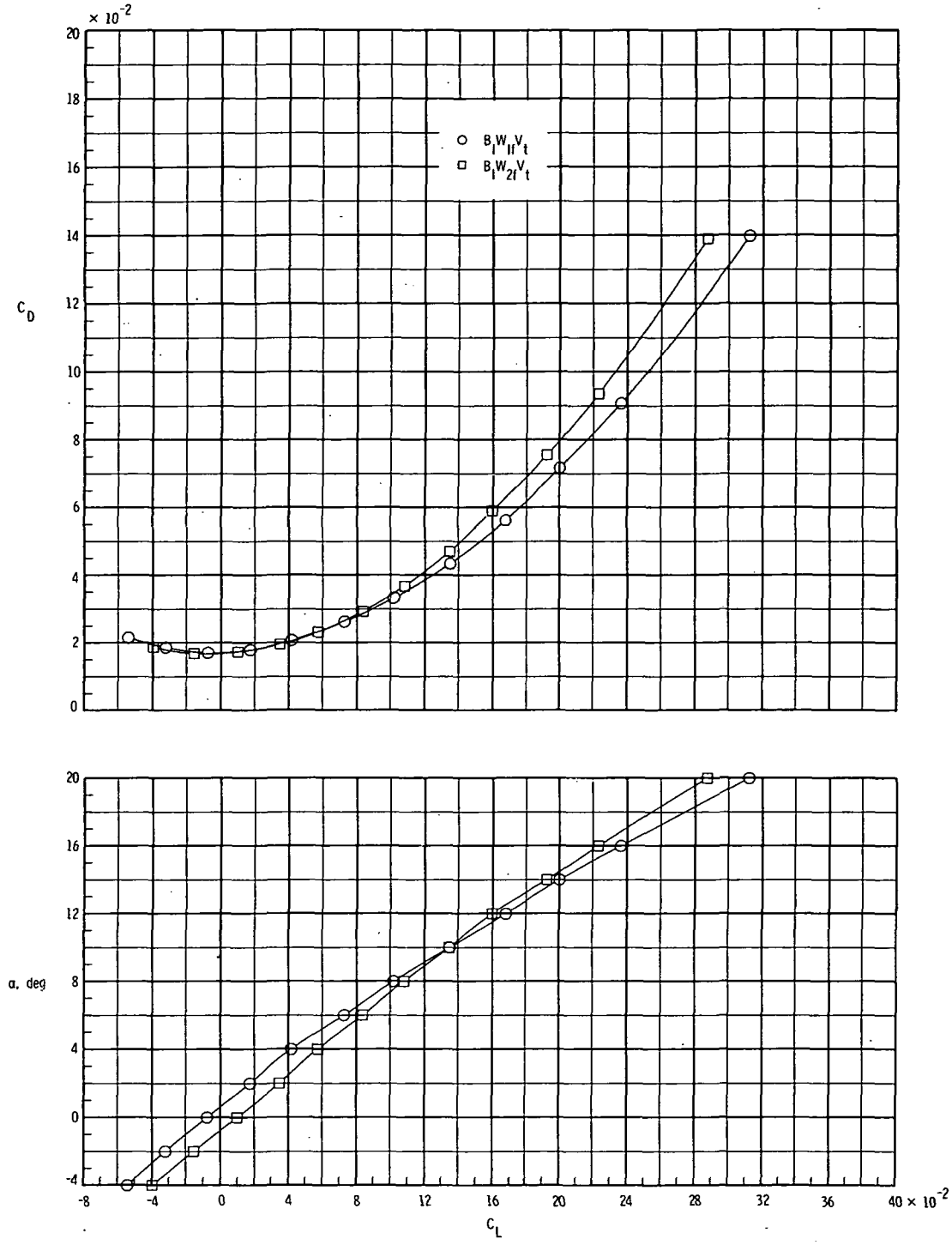


(b) Drag and lift.

Figure 9.- Concluded.

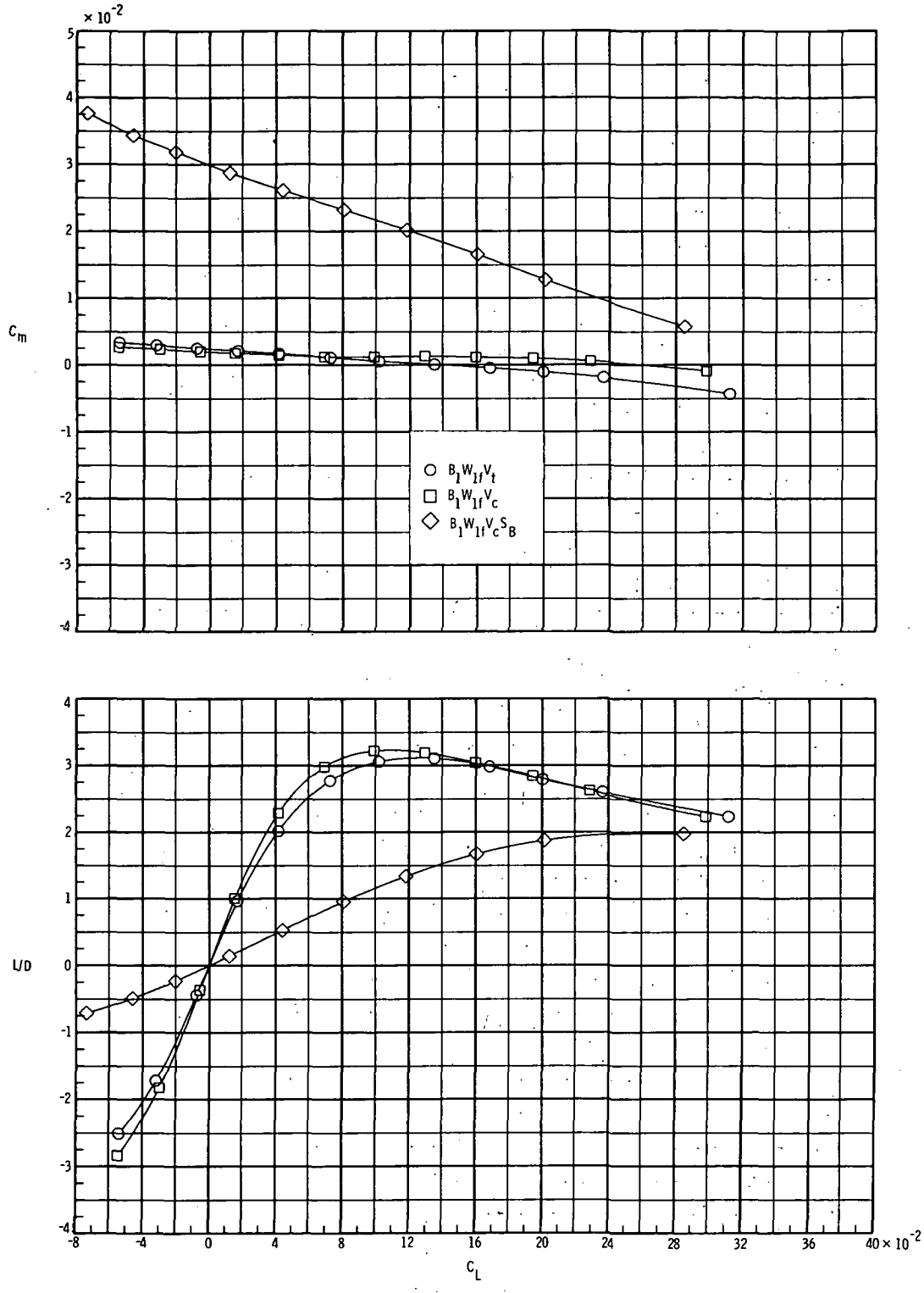


(a) Pitch and lift-drag ratio.

Figure 10.- Effect of lateral-directional controls and speed brakes on longitudinal characteristics; $\delta = 0^{o}$.

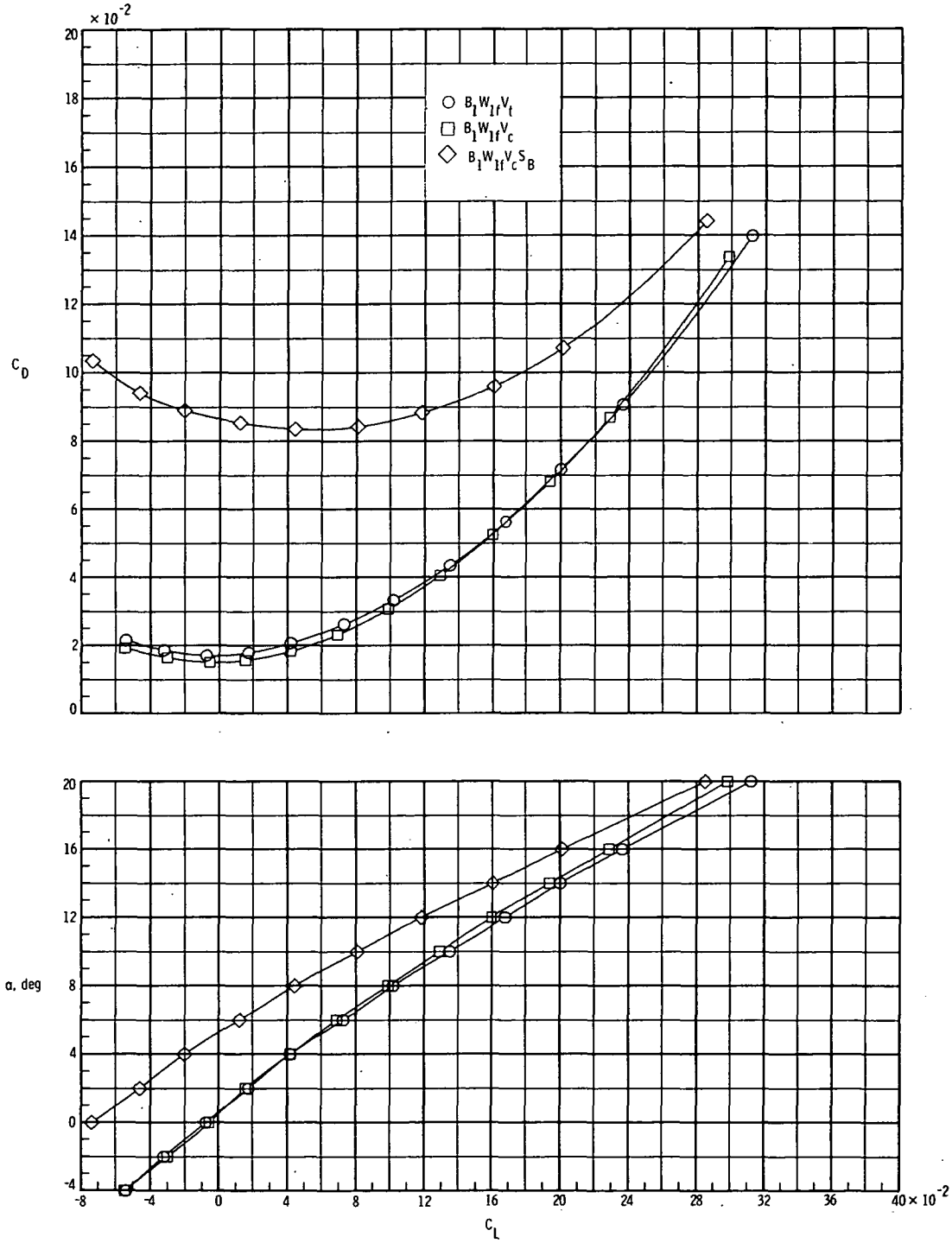


(b) Drag and lift.

Figure 10.- Concluded.

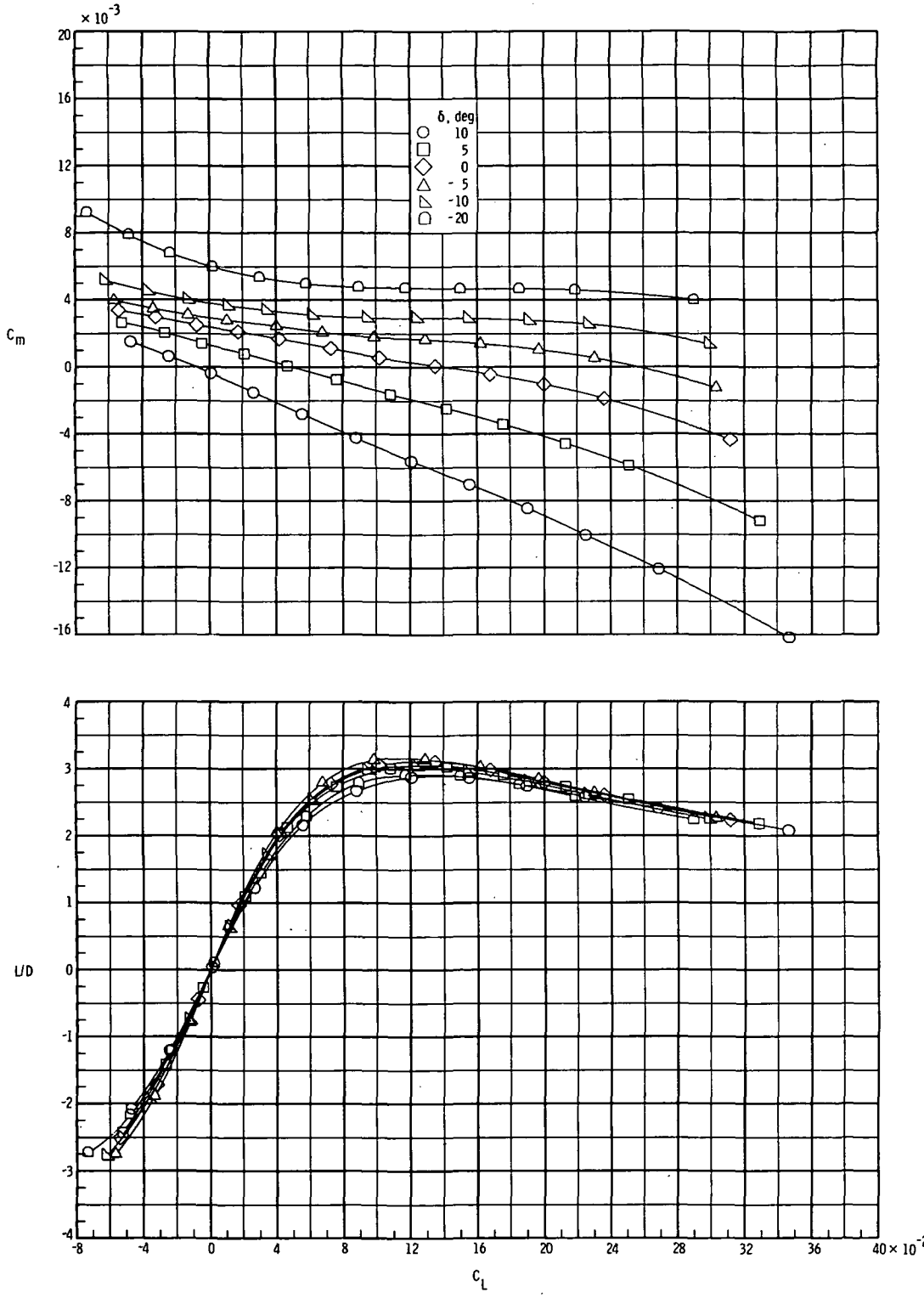


(a) Pitch and lift-drag ratio.

Figure 11.- Effect of elevon deflections on longitudinal aerodynamic characteristics for configuration $B_1W_{1f}V_t$.

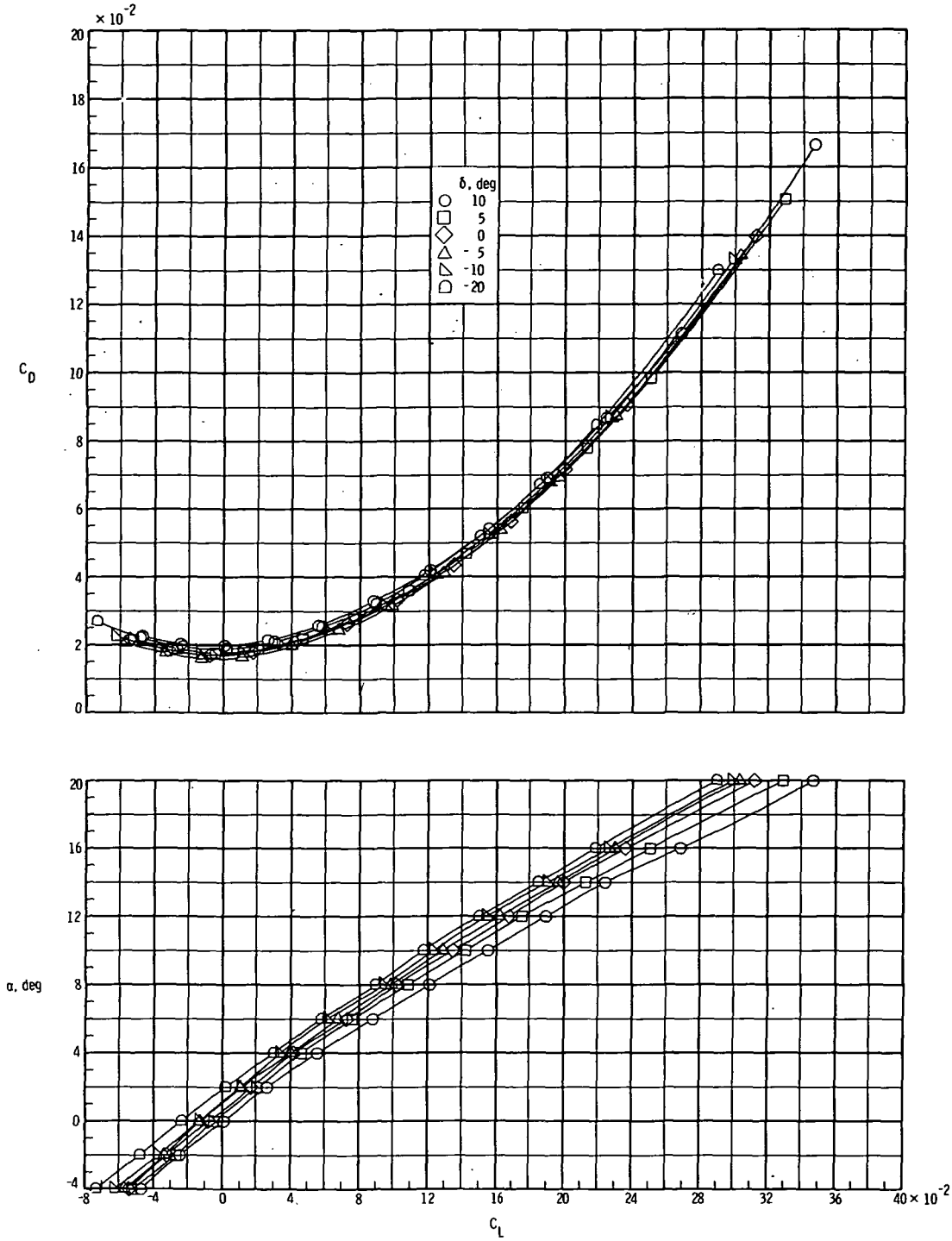


(b) Drag and lift.

Figure 11.- Concluded.

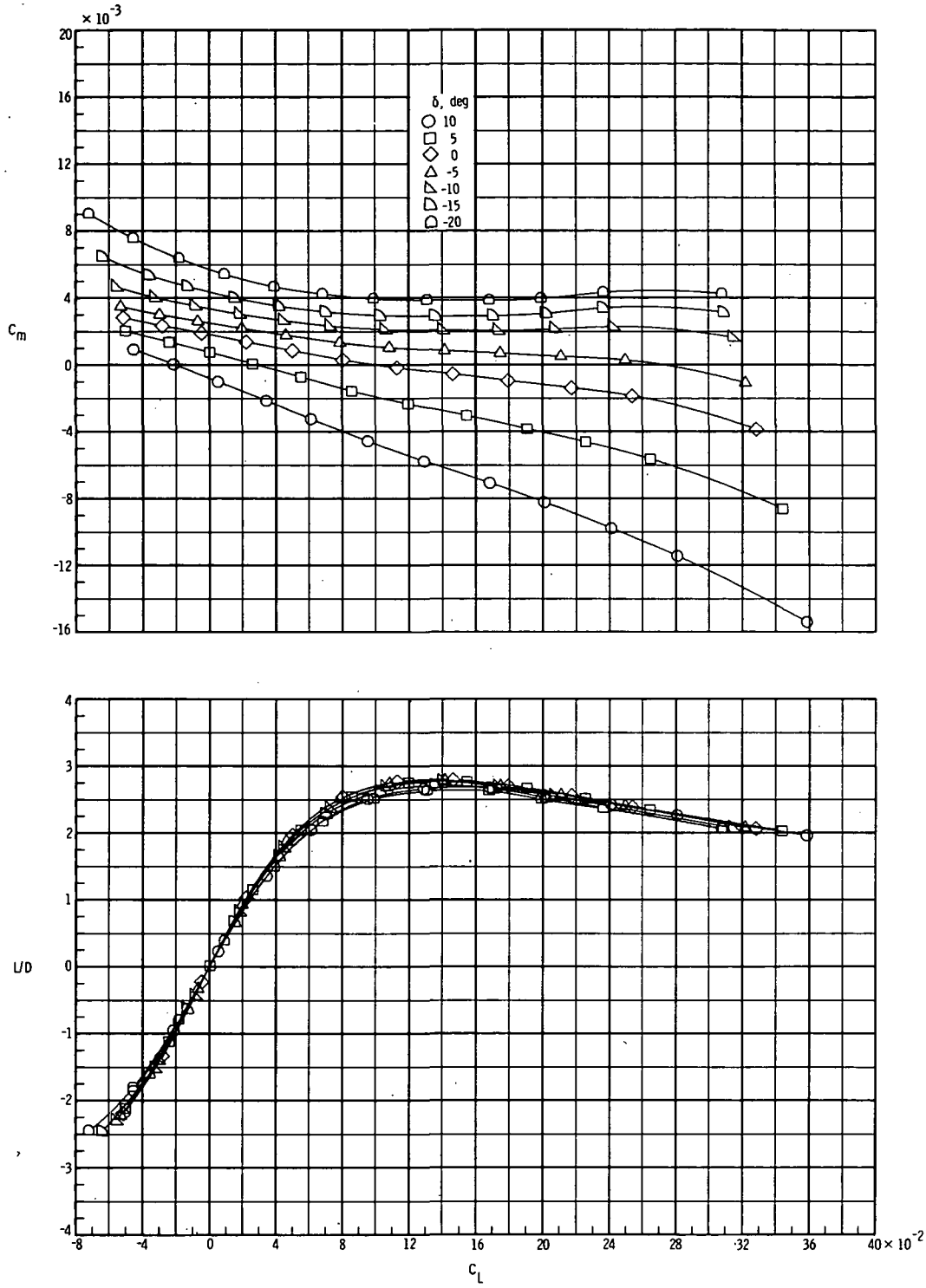


(a) Pitch and lift-drag ratio.

Figure 12.- Effect of elevon deflections on longitudinal aerodynamic characteristics for configuration $B_1W_{1f}V_tE$.

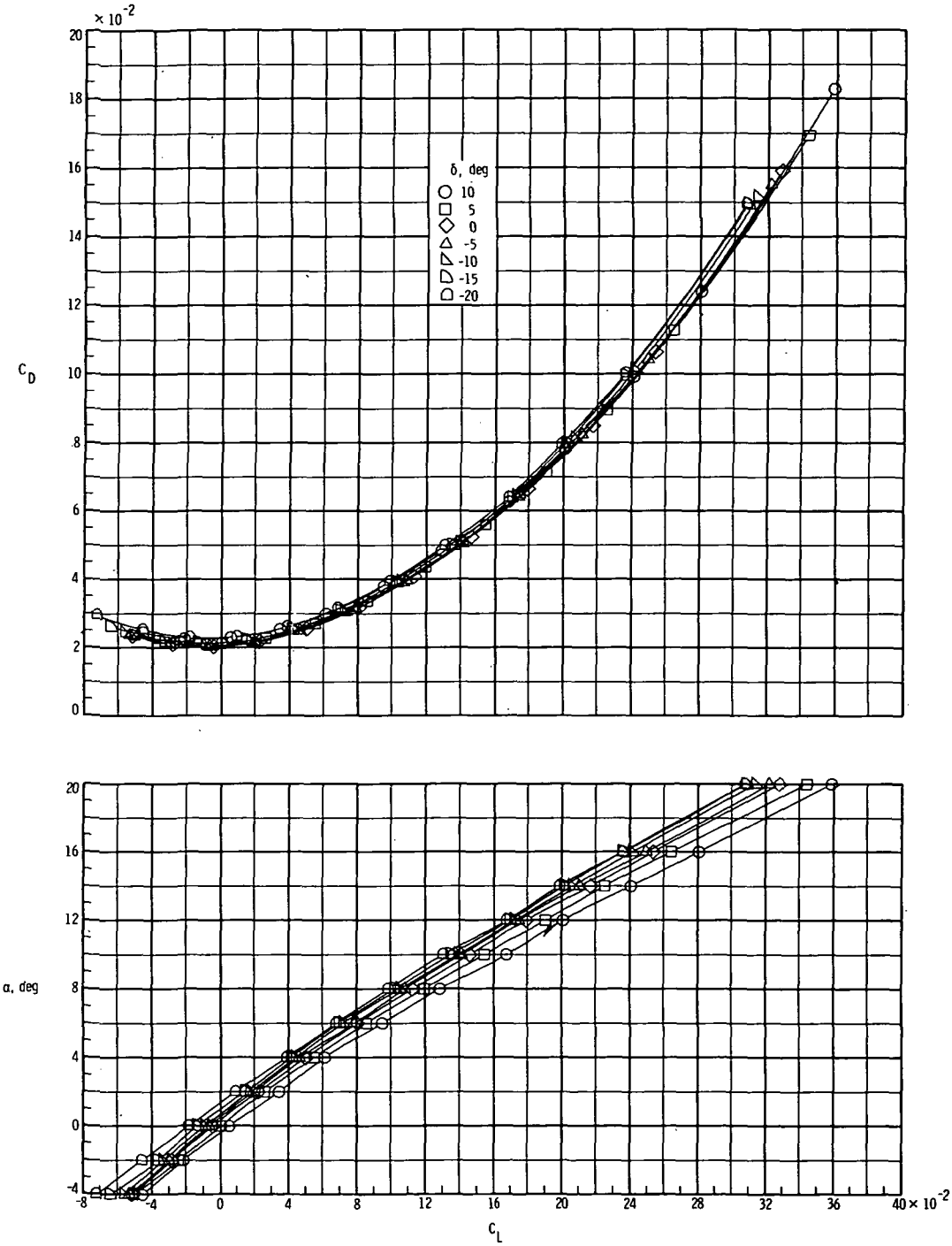


(b) Drag and lift.

Figure 12.- Concluded.

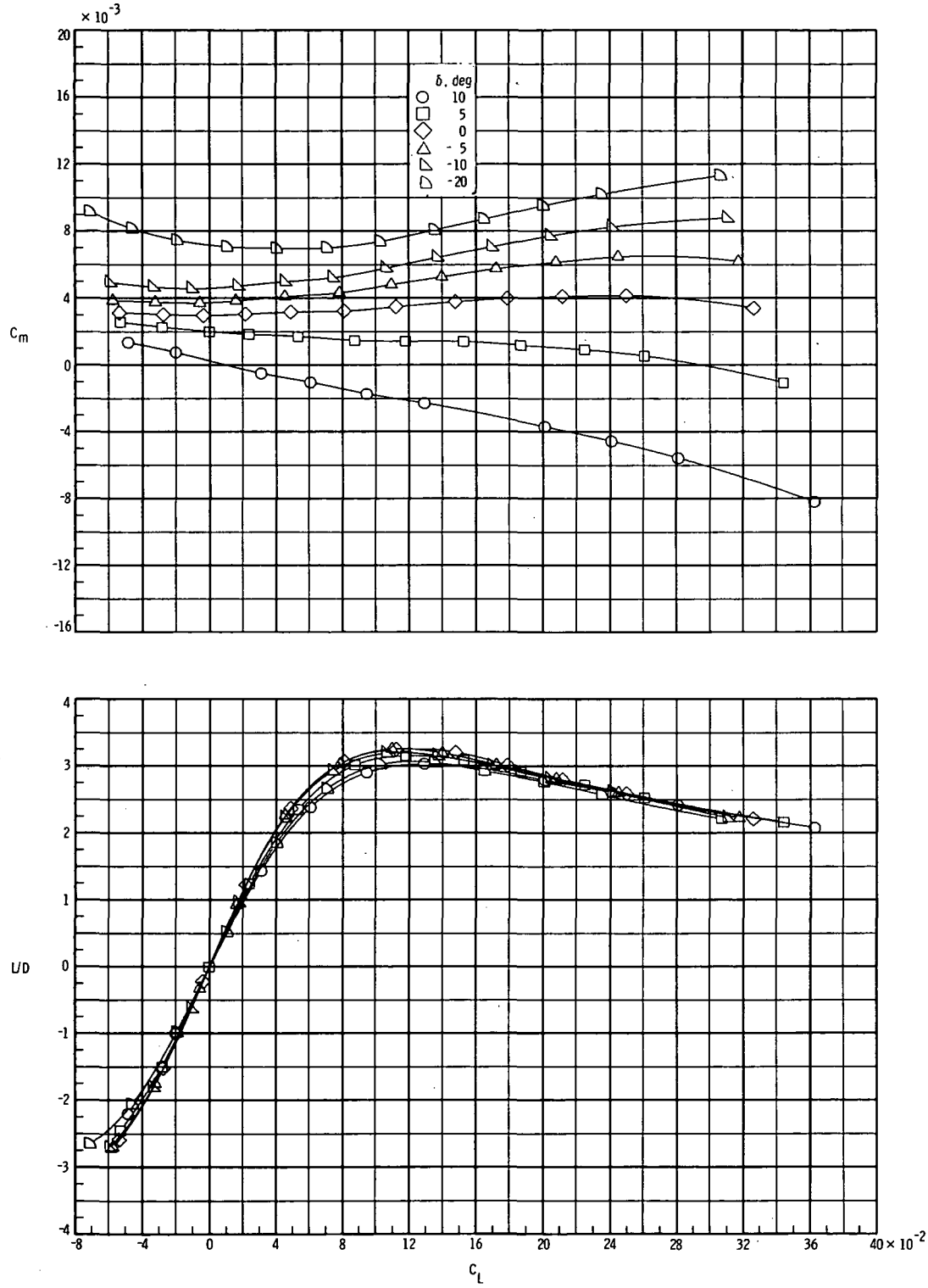


(a) Pitch and lift-drag ratio.

Figure 13.- Effect of elevon deflection on longitudinal aerodynamic characteristics for configuration $B_1W_{1f}V_tF_D$.

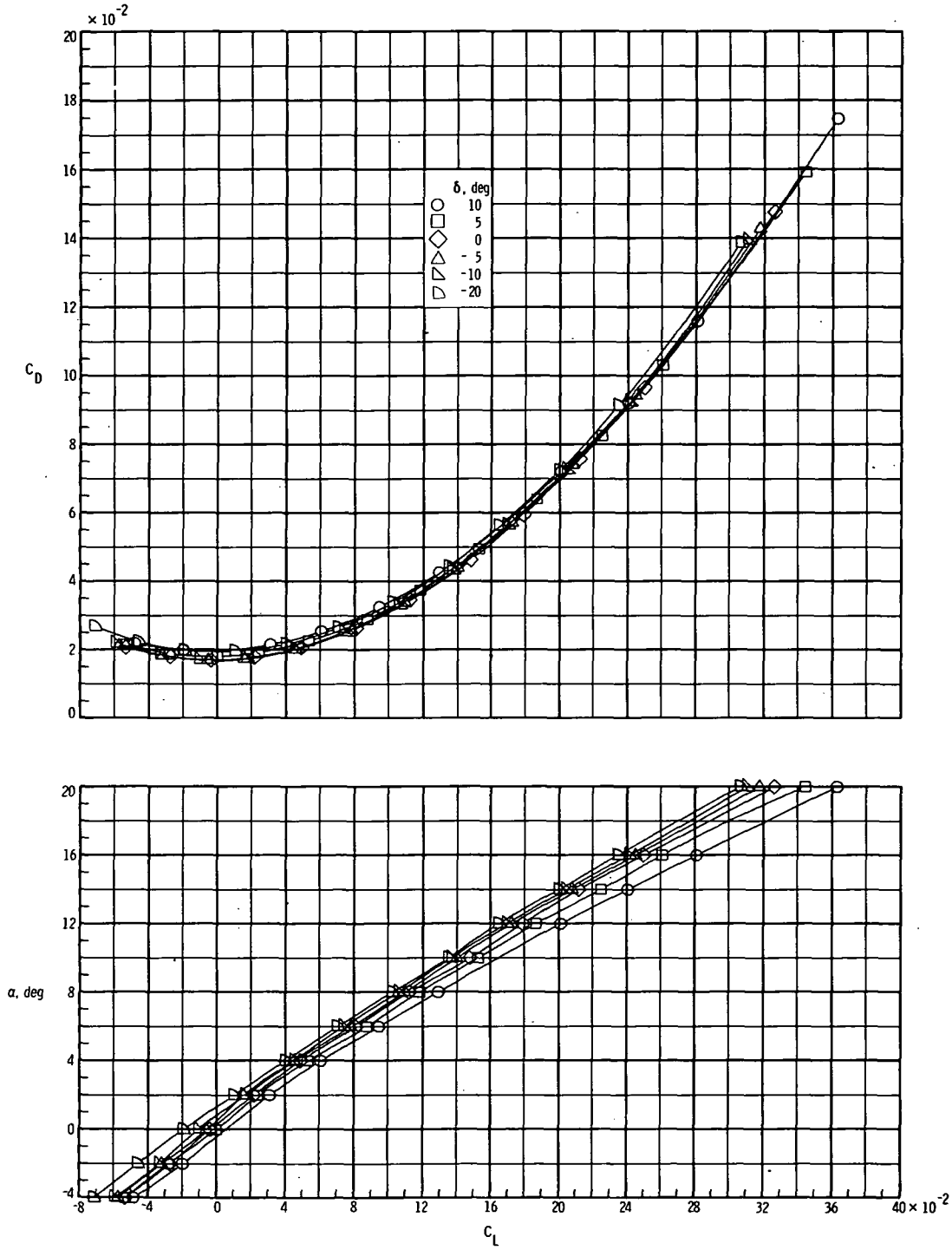


(b) Drag and lift.

Figure 13.- Concluded.

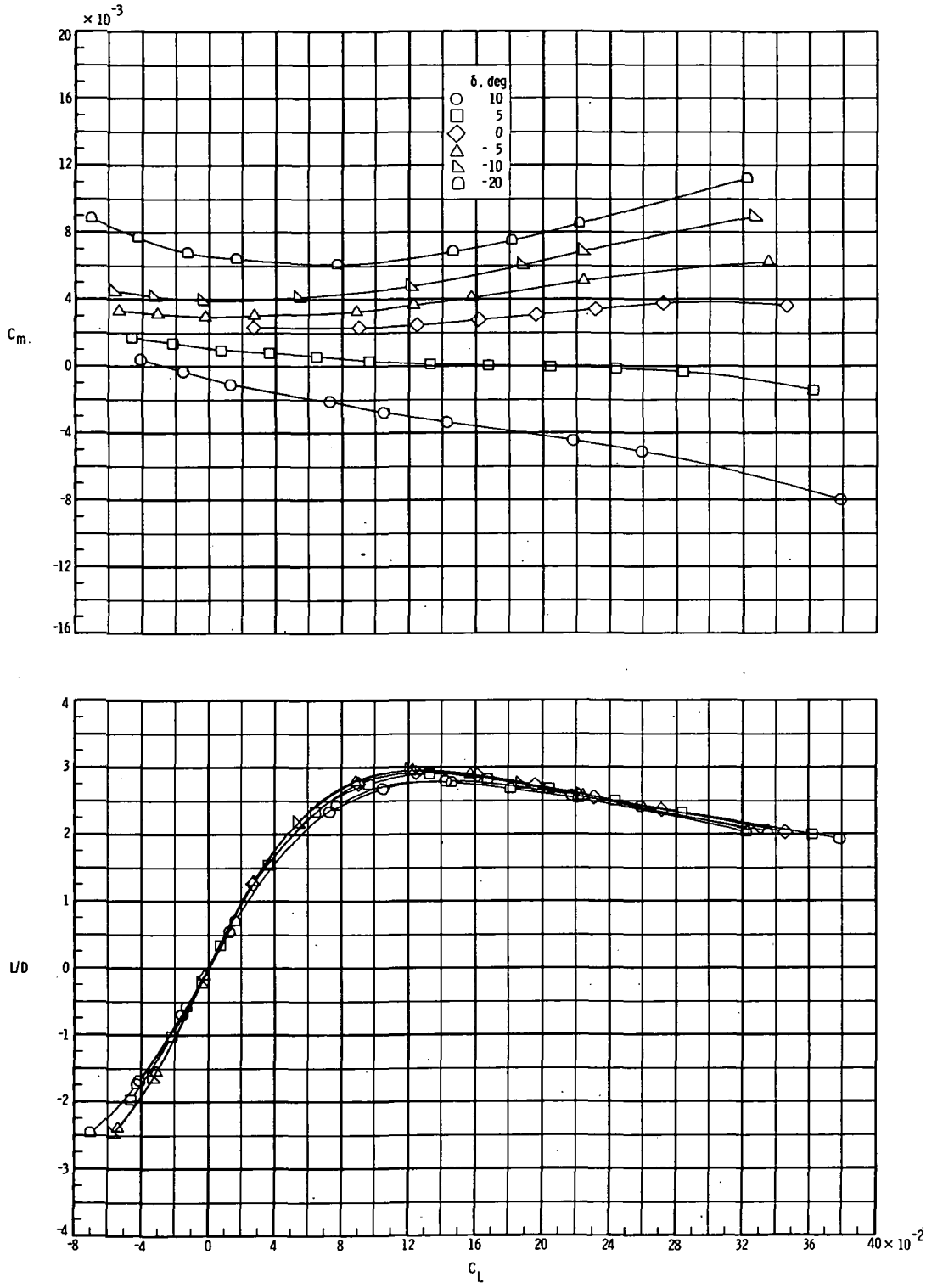


(a) Pitch and lift-drag ratio.

Figure 14.- Effect of elevon deflection on longitudinal aerodynamic characteristics for configuration $B_1W_{1f}V_tF_DE$.

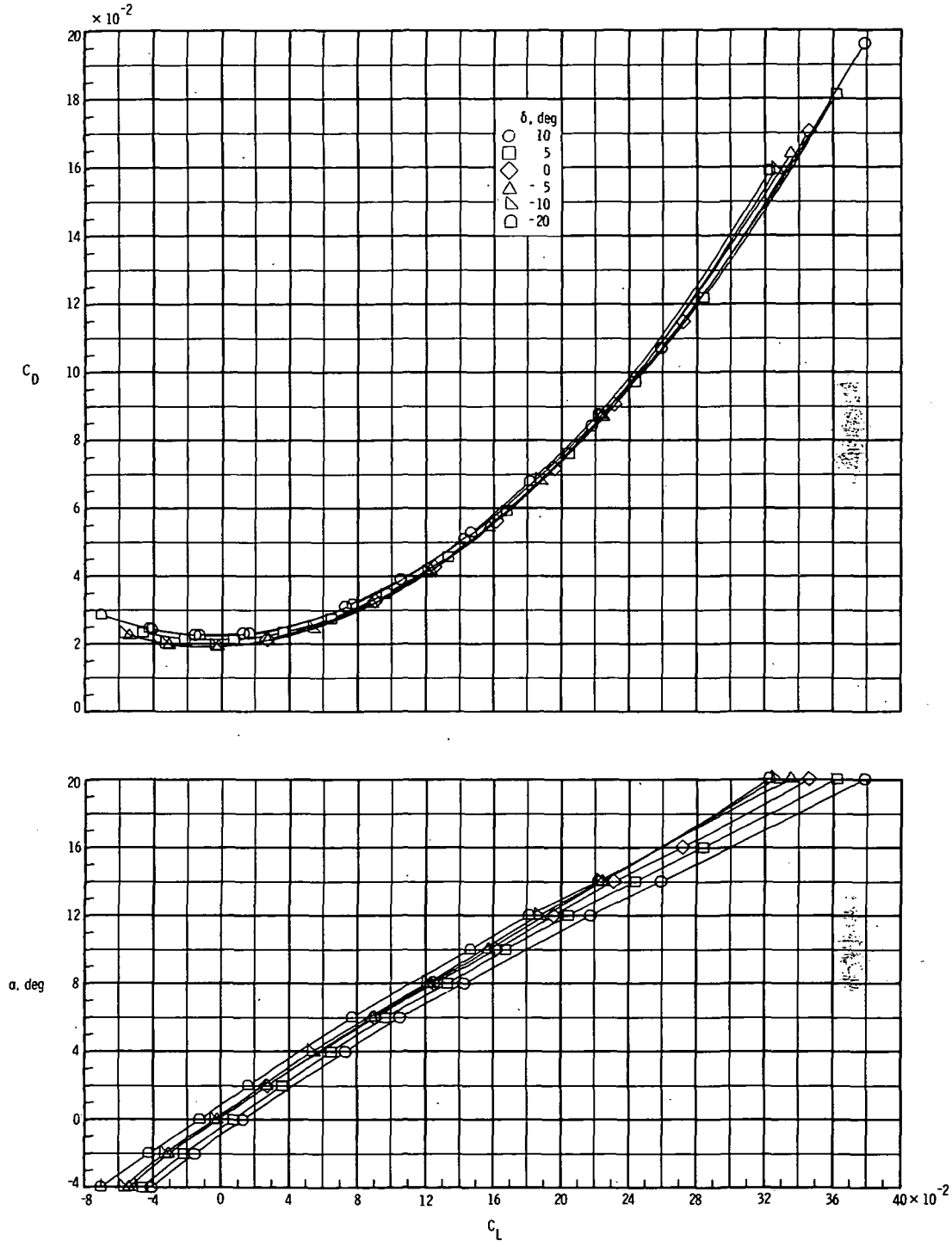


(b) Drag and lift.

Figure 14.- Concluded.

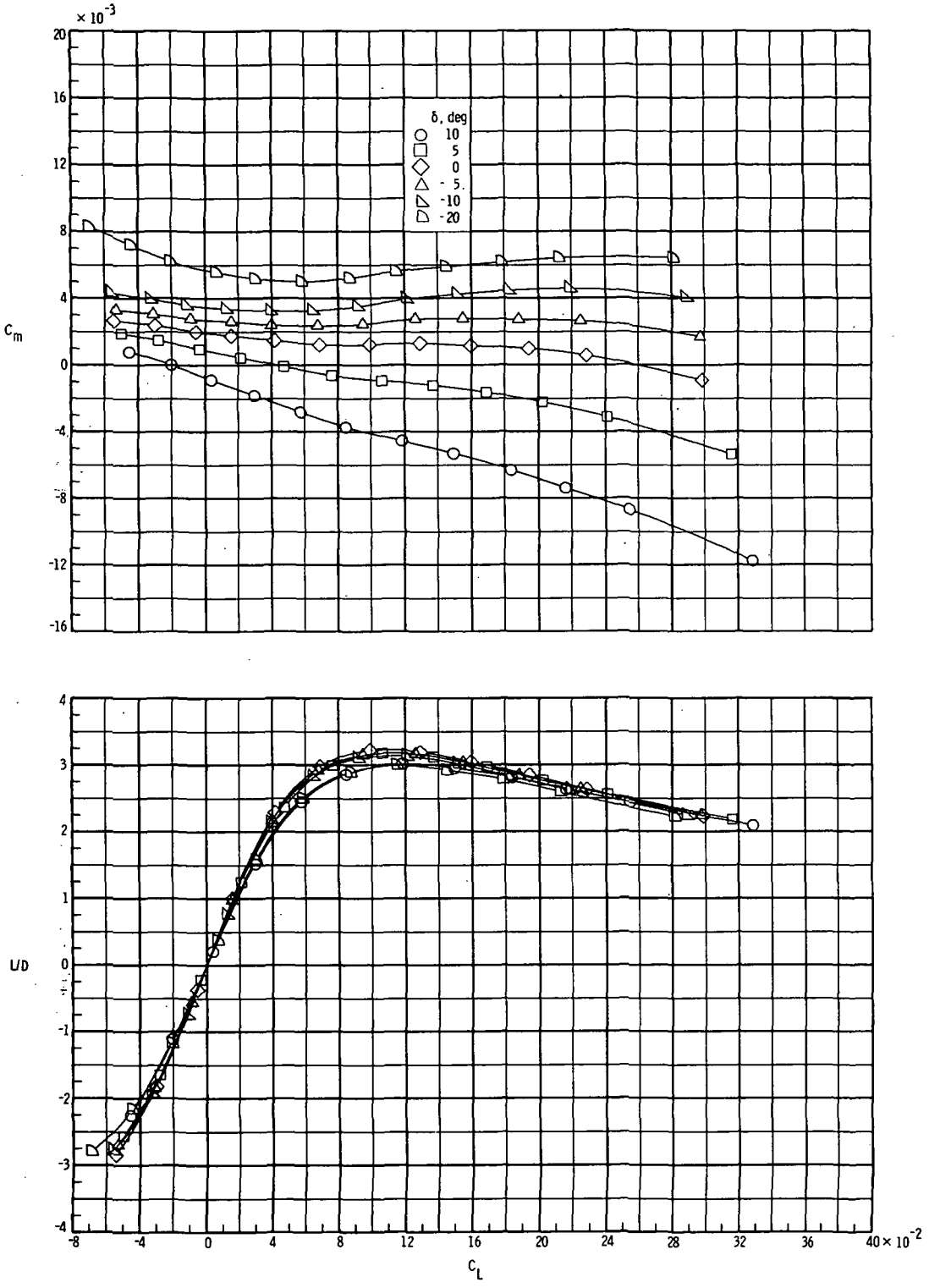


(a) Pitch and lift-drag ratio.

Figure 15.- Effect of elevon deflections on longitudinal aerodynamic characteristics for configuration $B_1W_{1f}V_c$.

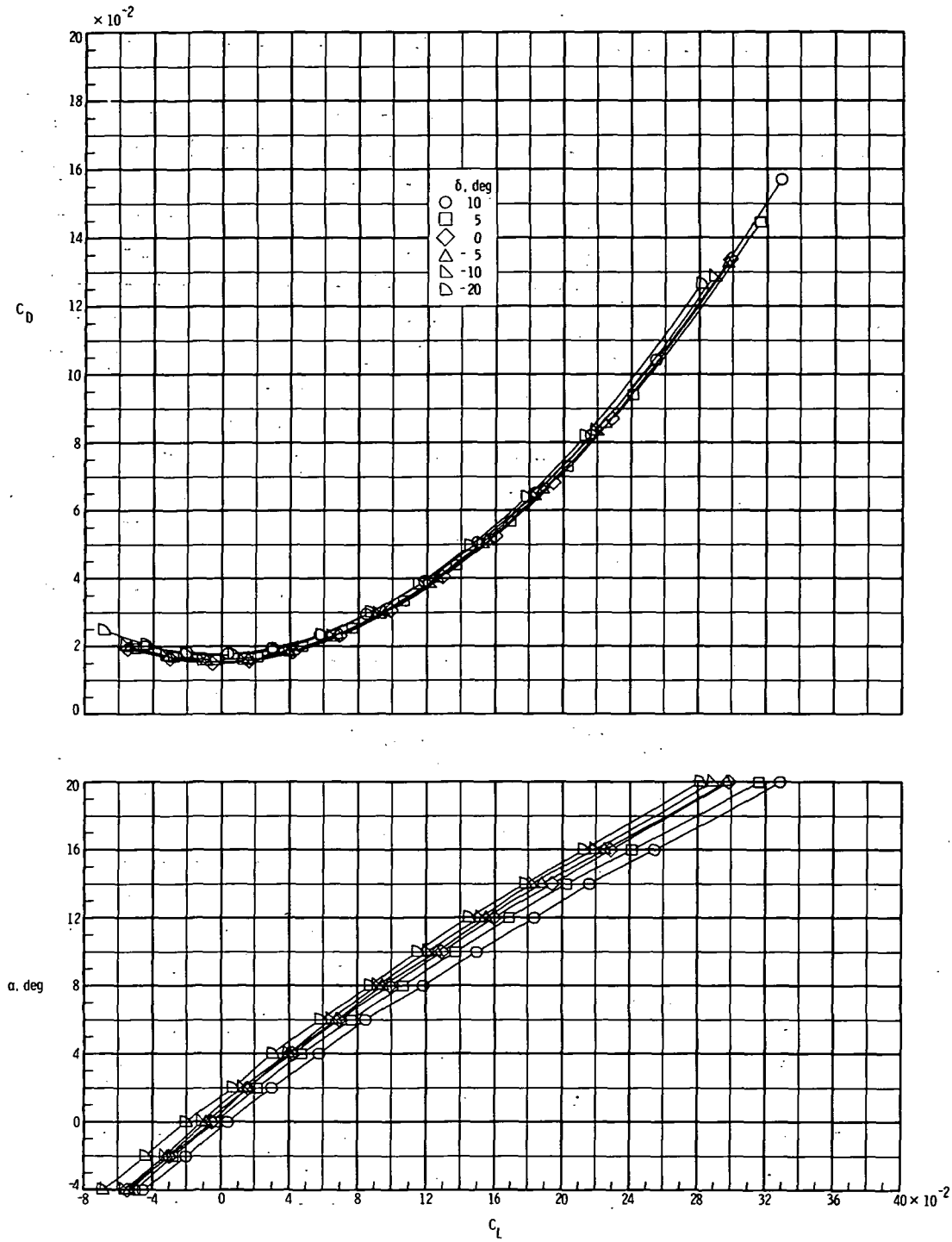


(b) Drag and lift.

Figure 15.- Concluded.

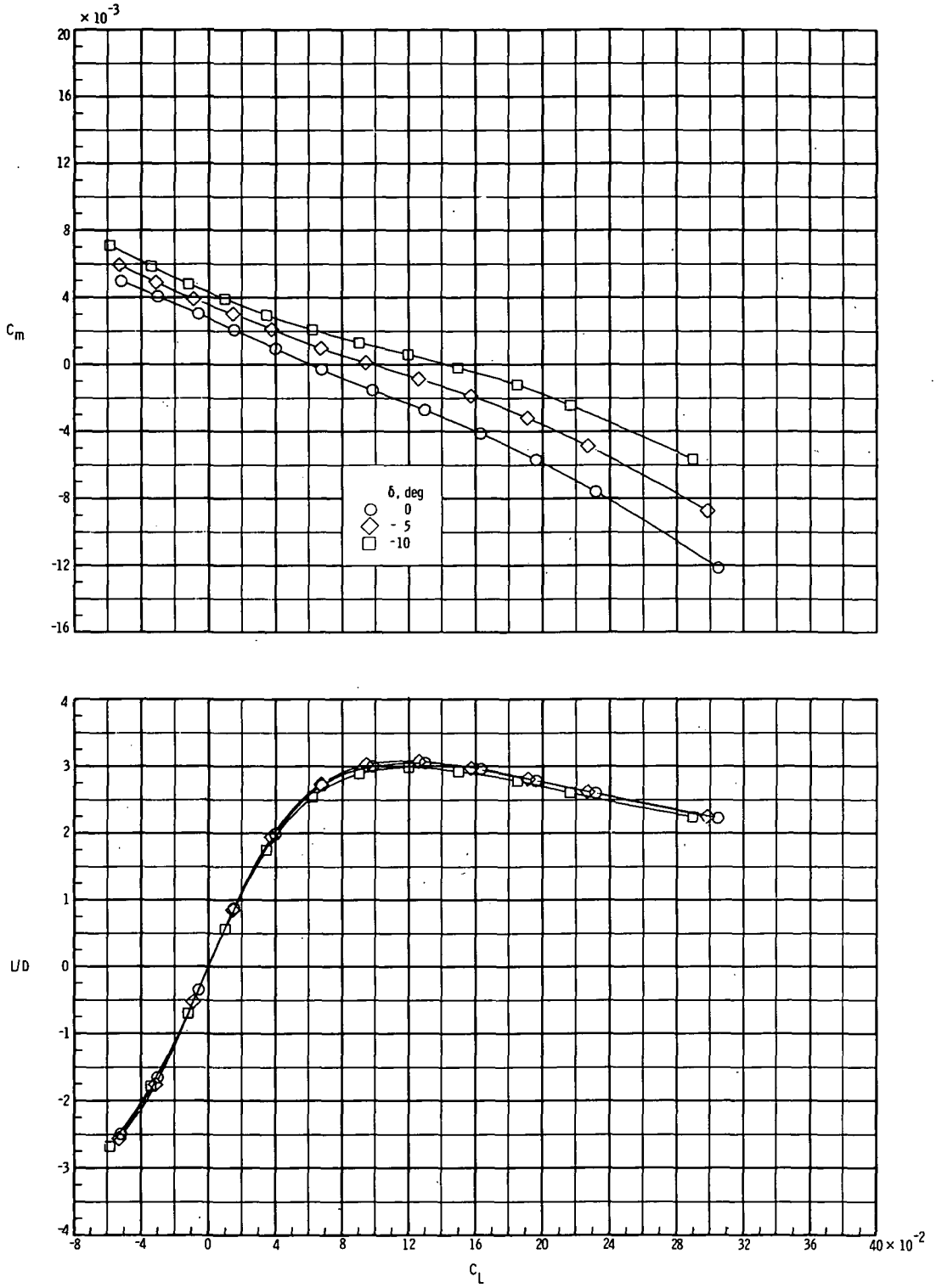


(a) Pitch and lift-drag ratio.

Figure 16.- Effect of elevon deflections on longitudinal aerodynamic characteristics for configuration $B_1W_{1a}V_c$.

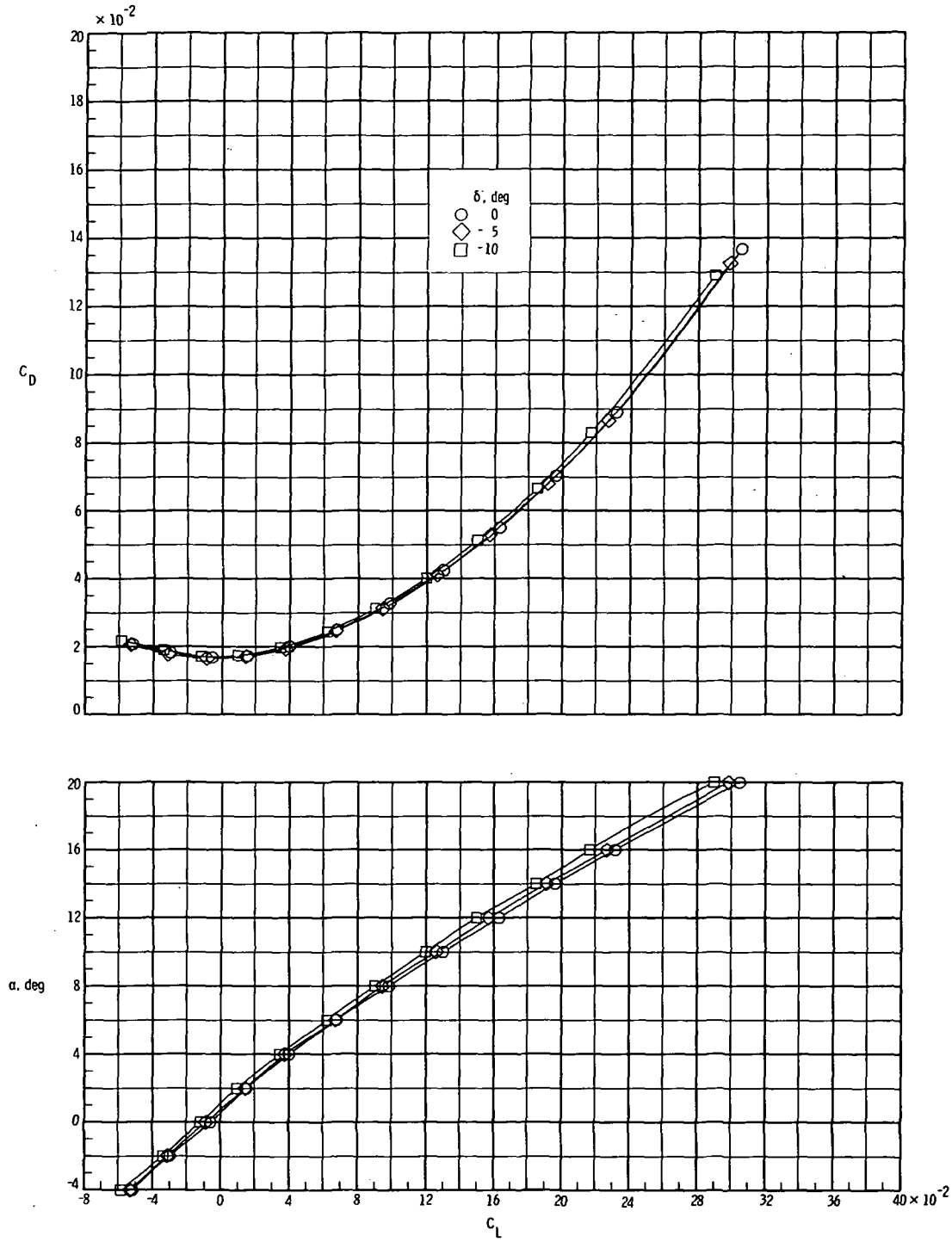


(b) Drag and lift.

Figure 16.- Concluded.

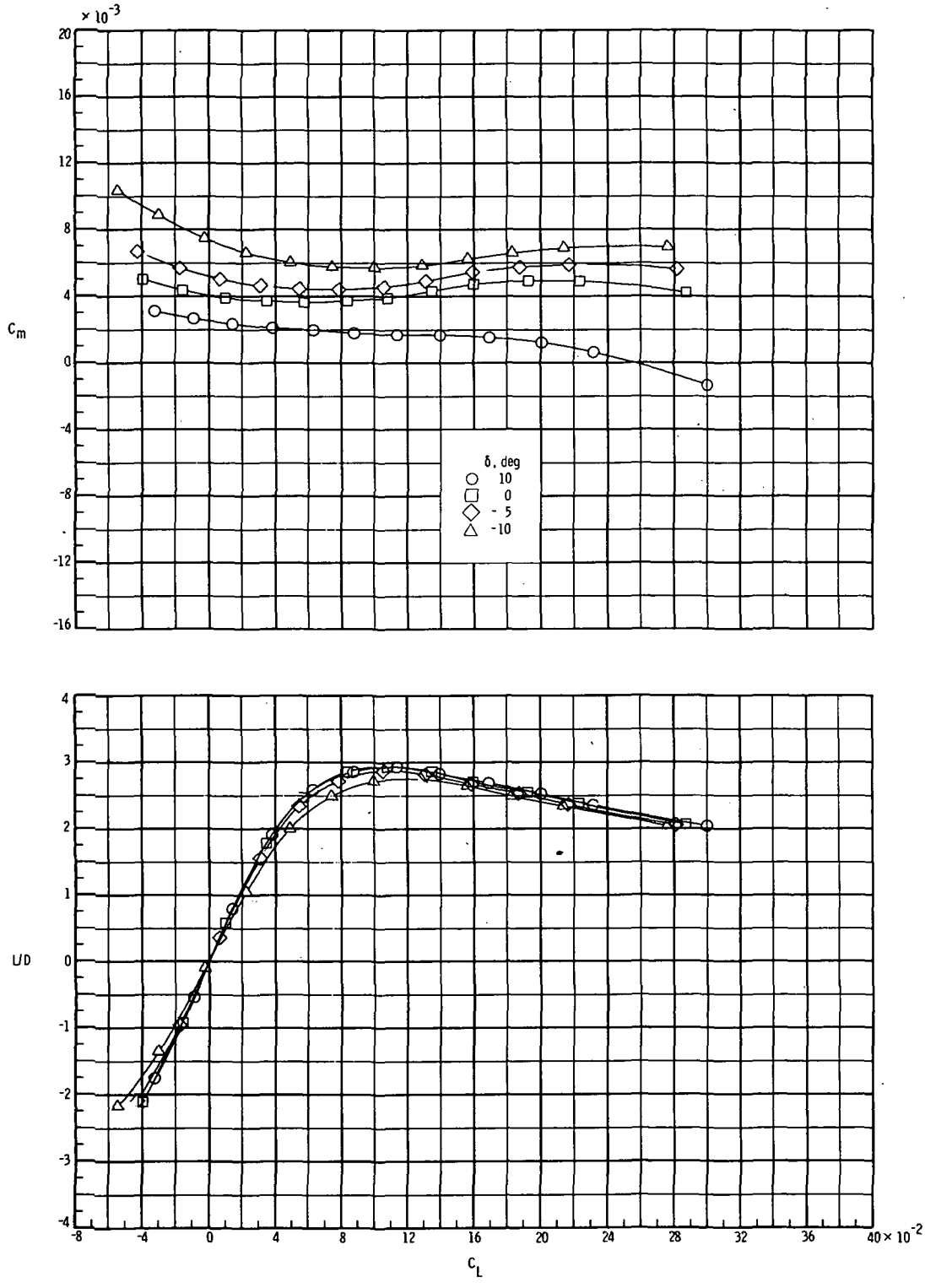


(a) Pitch and lift-drag ratio.

Figure 17.- Effect of elevon deflections on longitudinal aerodynamic characteristics for configuration $B_1W_{2f}V_t$.

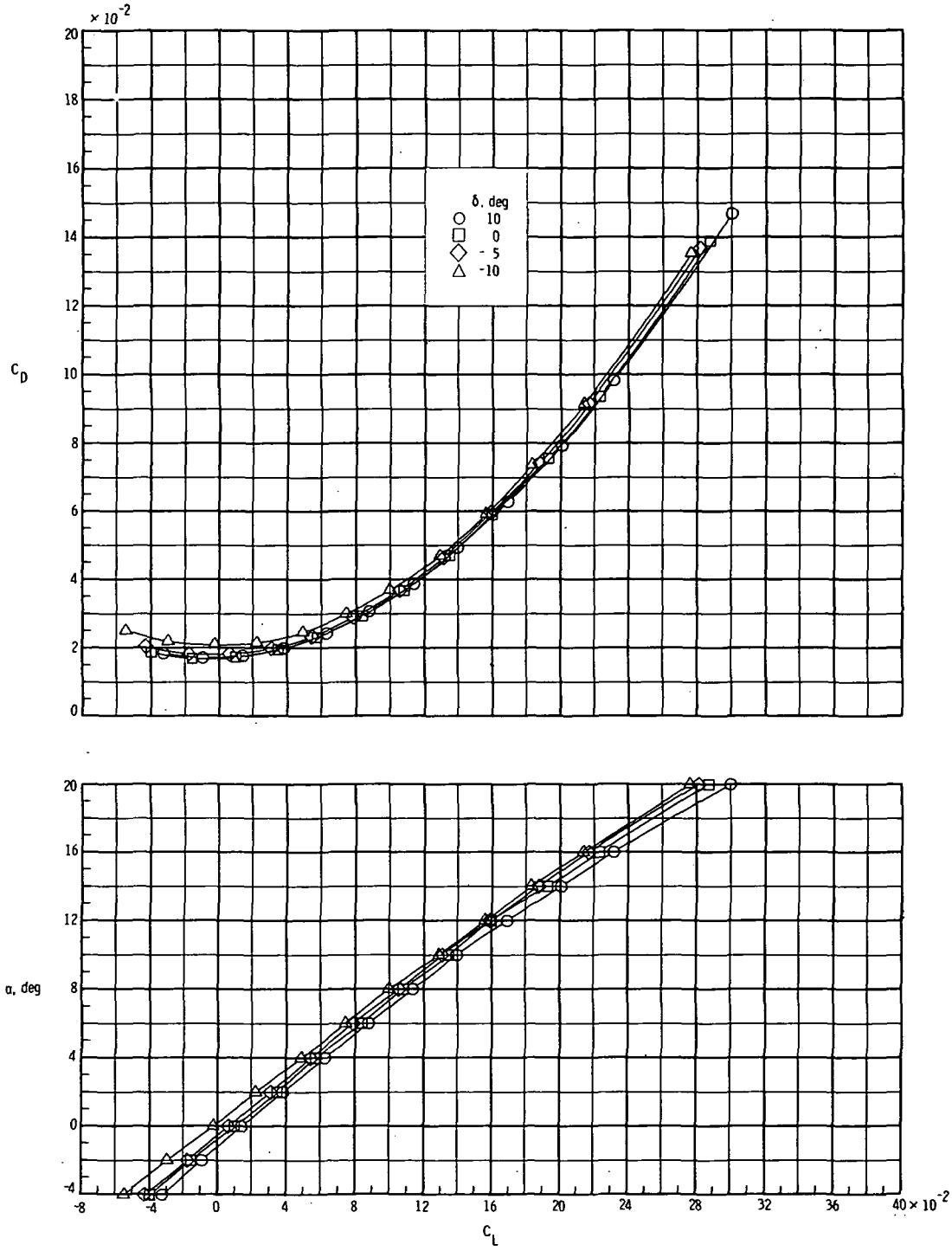


(b) Drag and lift.

Figure 17.- Concluded.

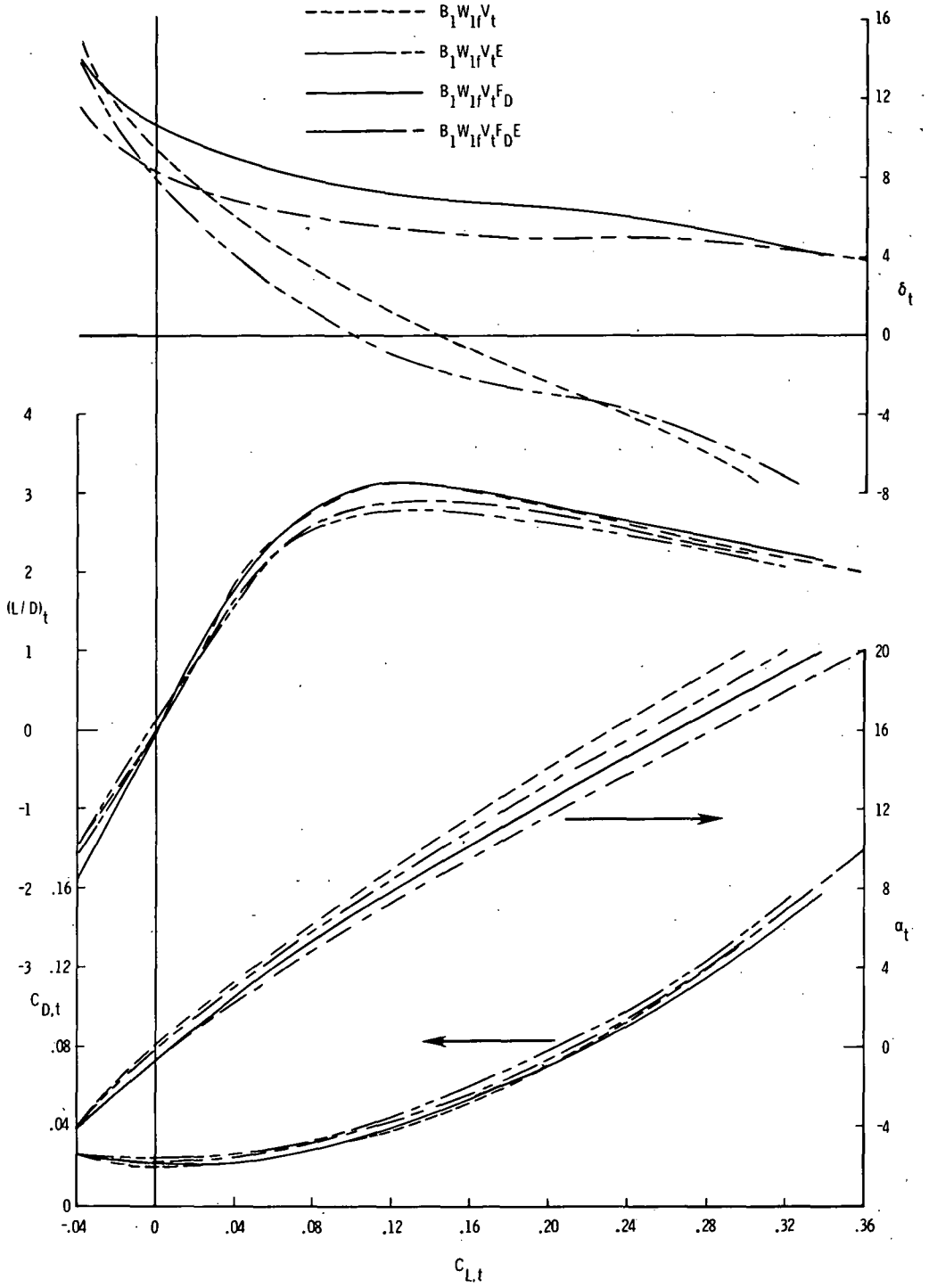


Figure 18.- Longitudinal trim characteristics for configurations $B_1W_{1f}V_t$, $B_1W_{1f}V_tE$, $B_1W_{1f}V_tF_D$, and $B_1W_{1f}V_tF_DE$.

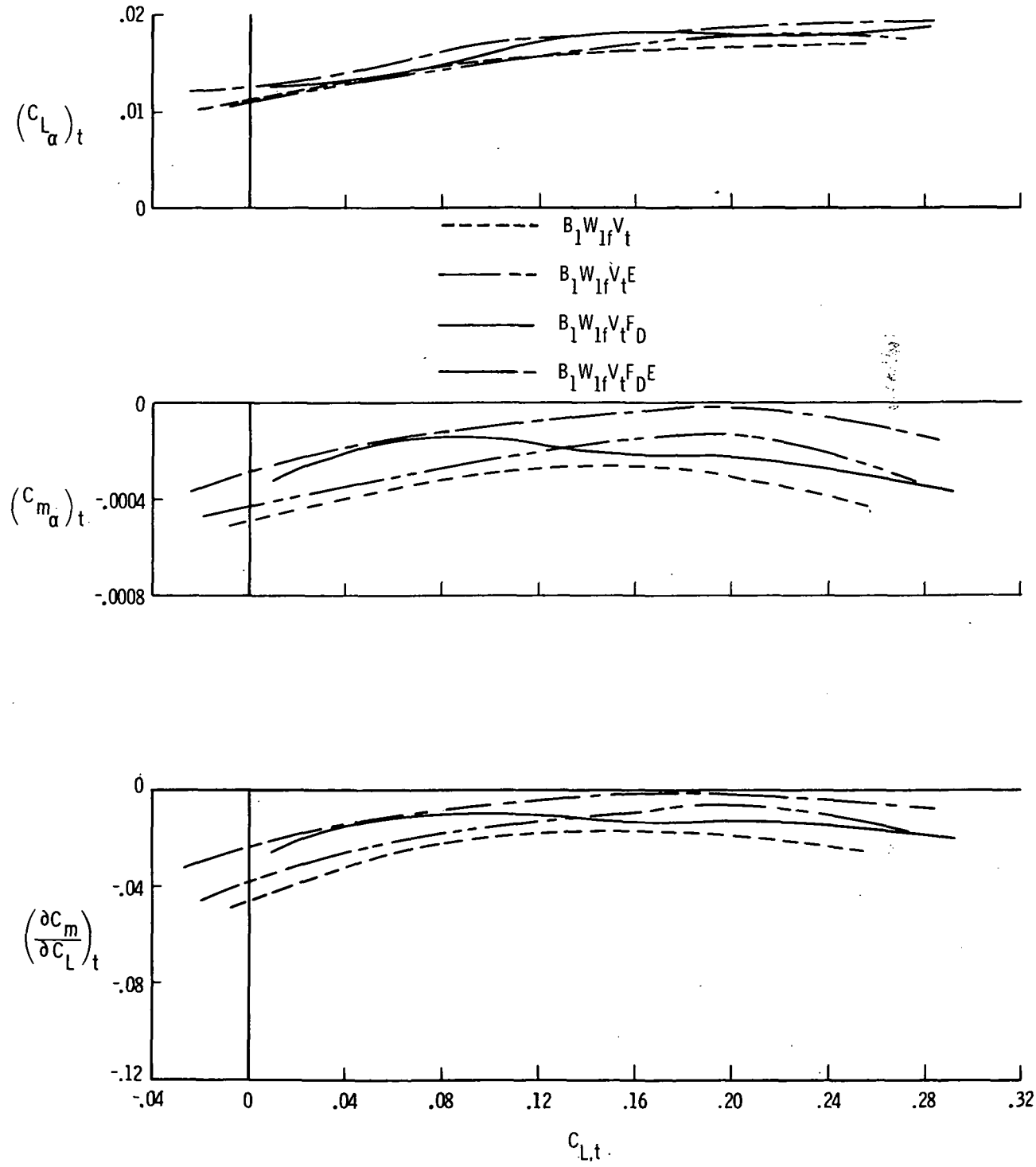


Figure 18.- Concluded.

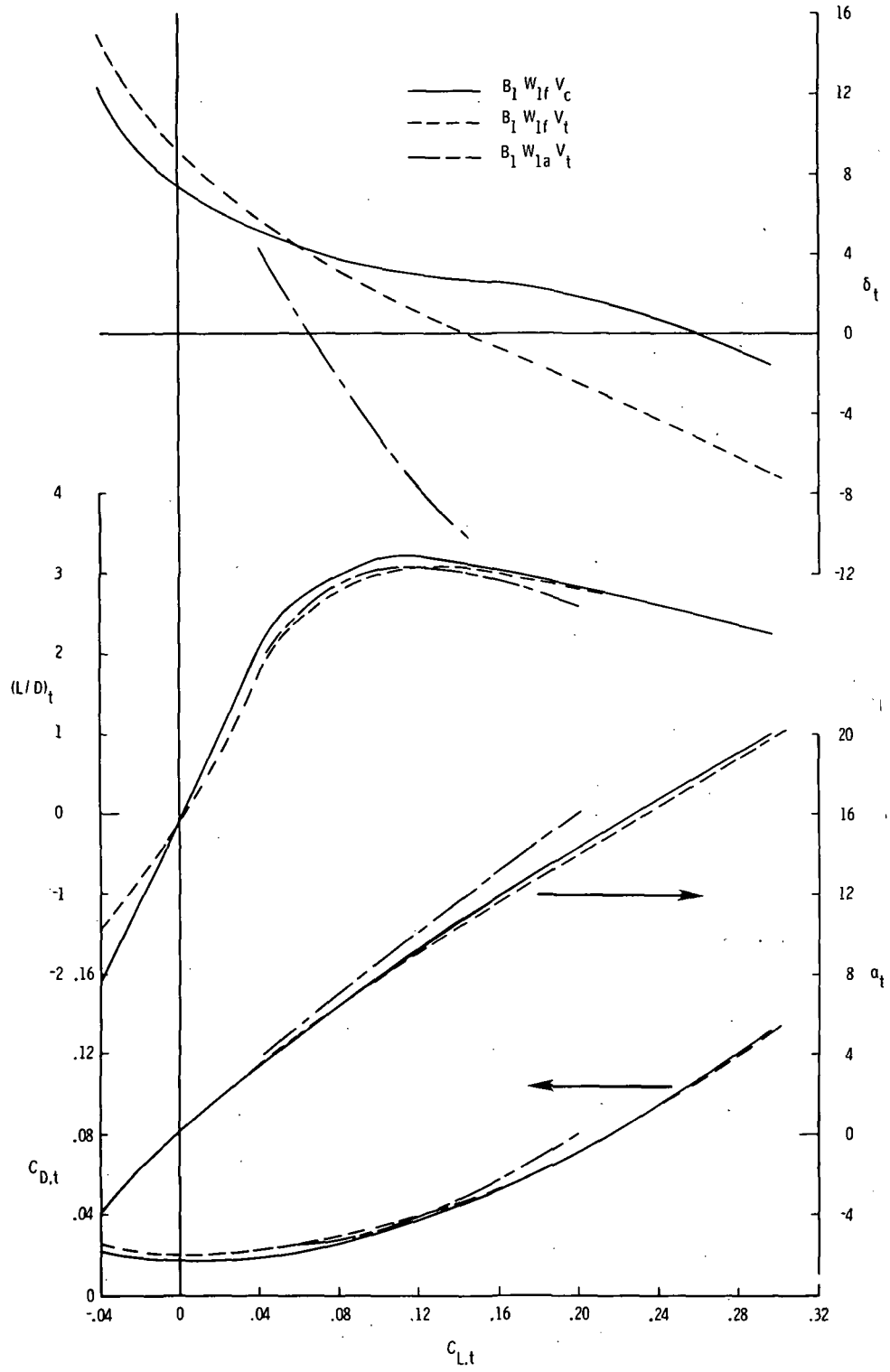


Figure 19.- Longitudinal trim characteristics for configurations $B_1W_{1f}V_c$, $B_1W_{1f}V_t$, and $B_1W_{1a}V_t$.

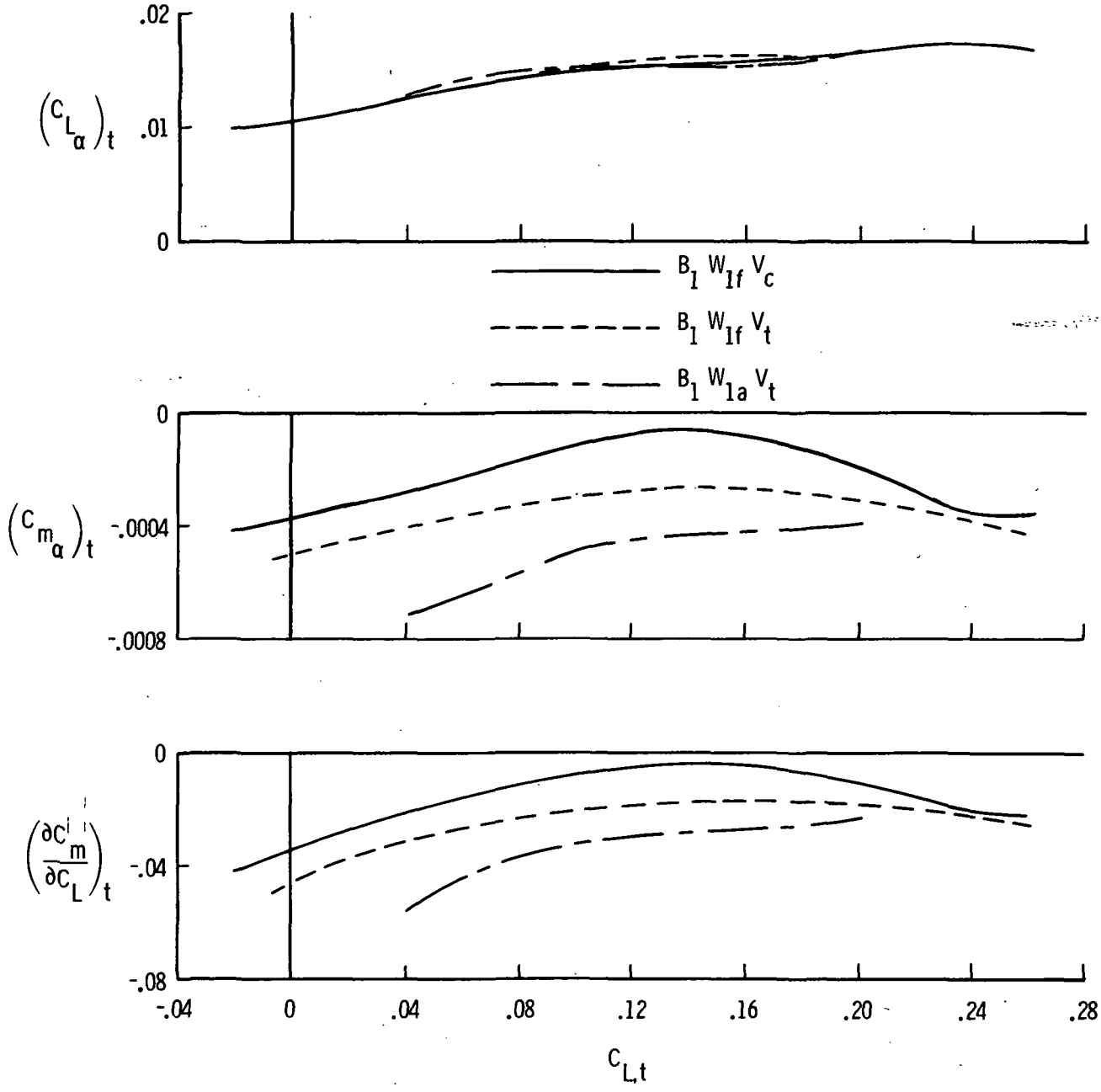


Figure 19.- Concluded.

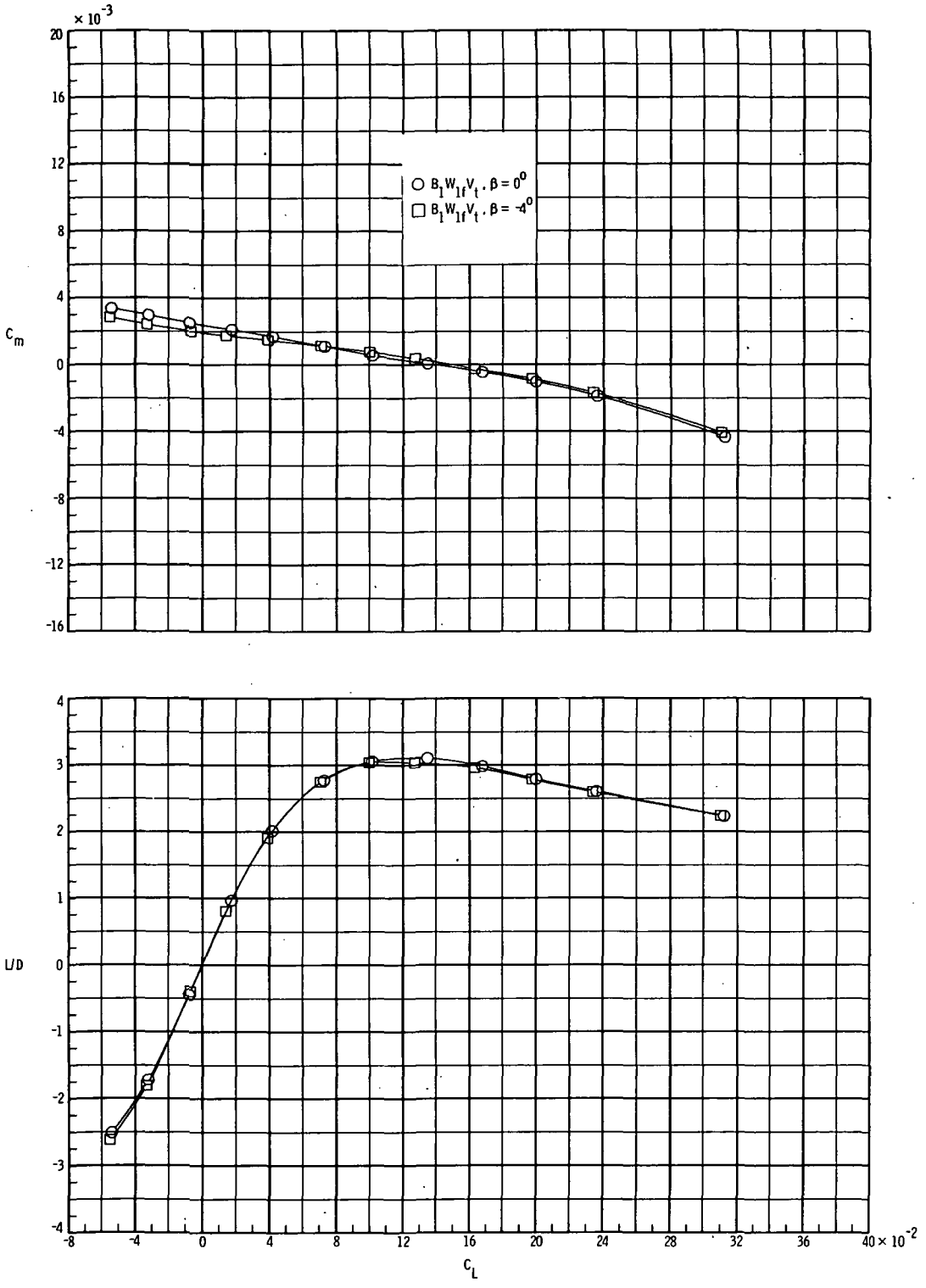


(a) Pitch and lift-drag ratio.

Figure 20.- Effect of sideslip on longitudinal characteristics for $\delta = 0^{\circ}$.

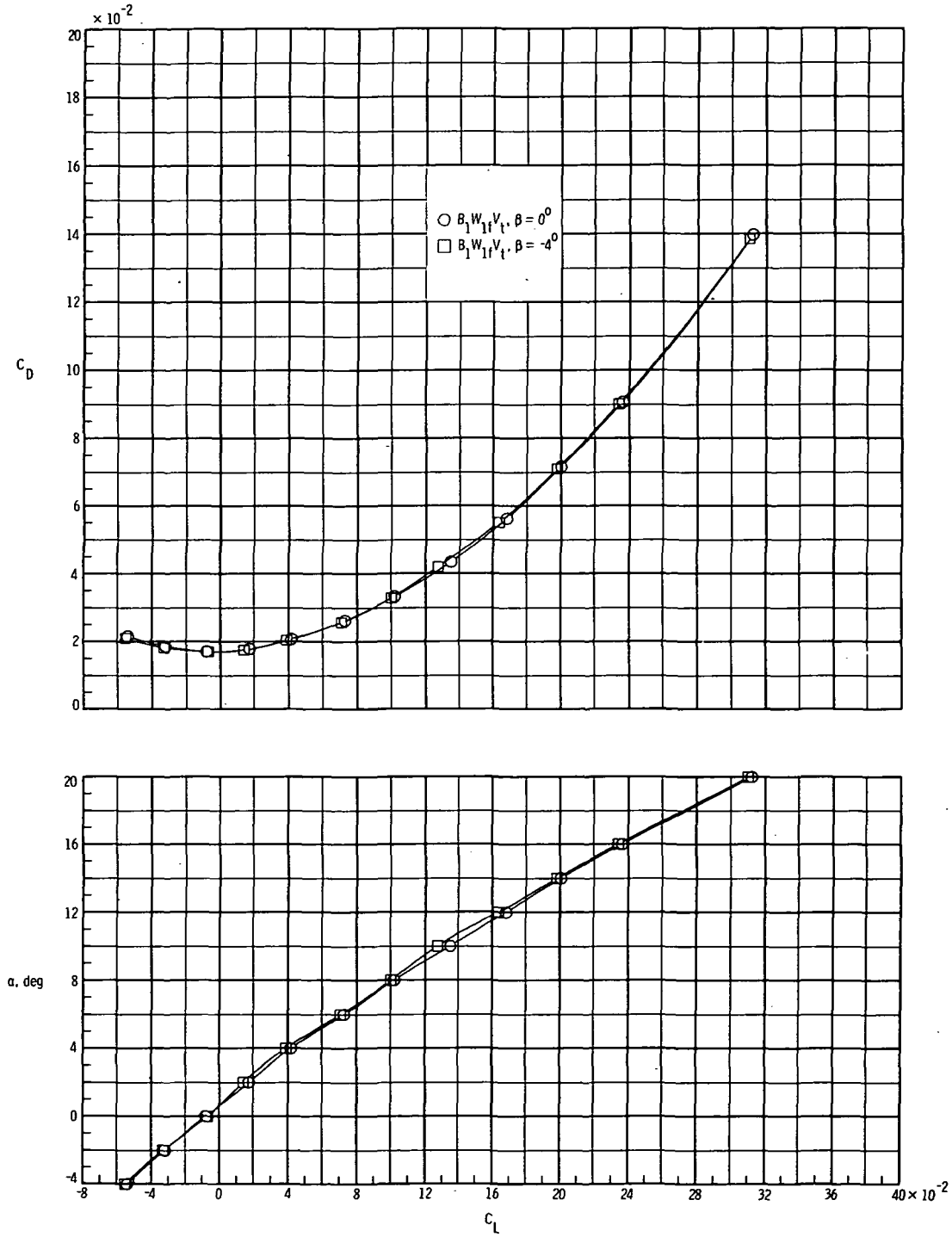


(b) Drag and lift.

Figure 20.- Concluded.

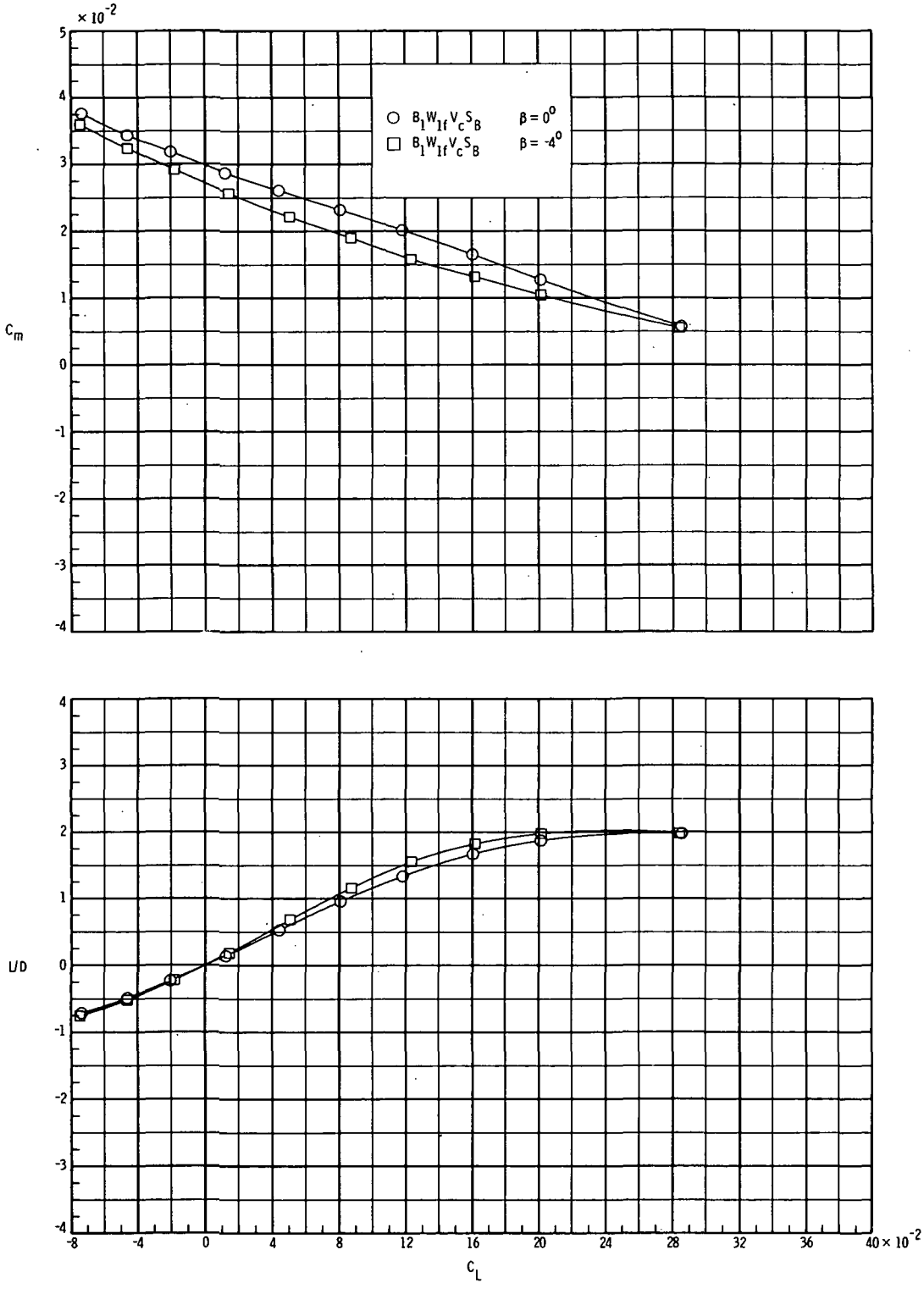


(a) Pitch and lift-drag ratio.

Figure 21.- Effect of sideslip on longitudinal characteristics of configuration with speed brakes for $\delta = 0^{\circ}$.

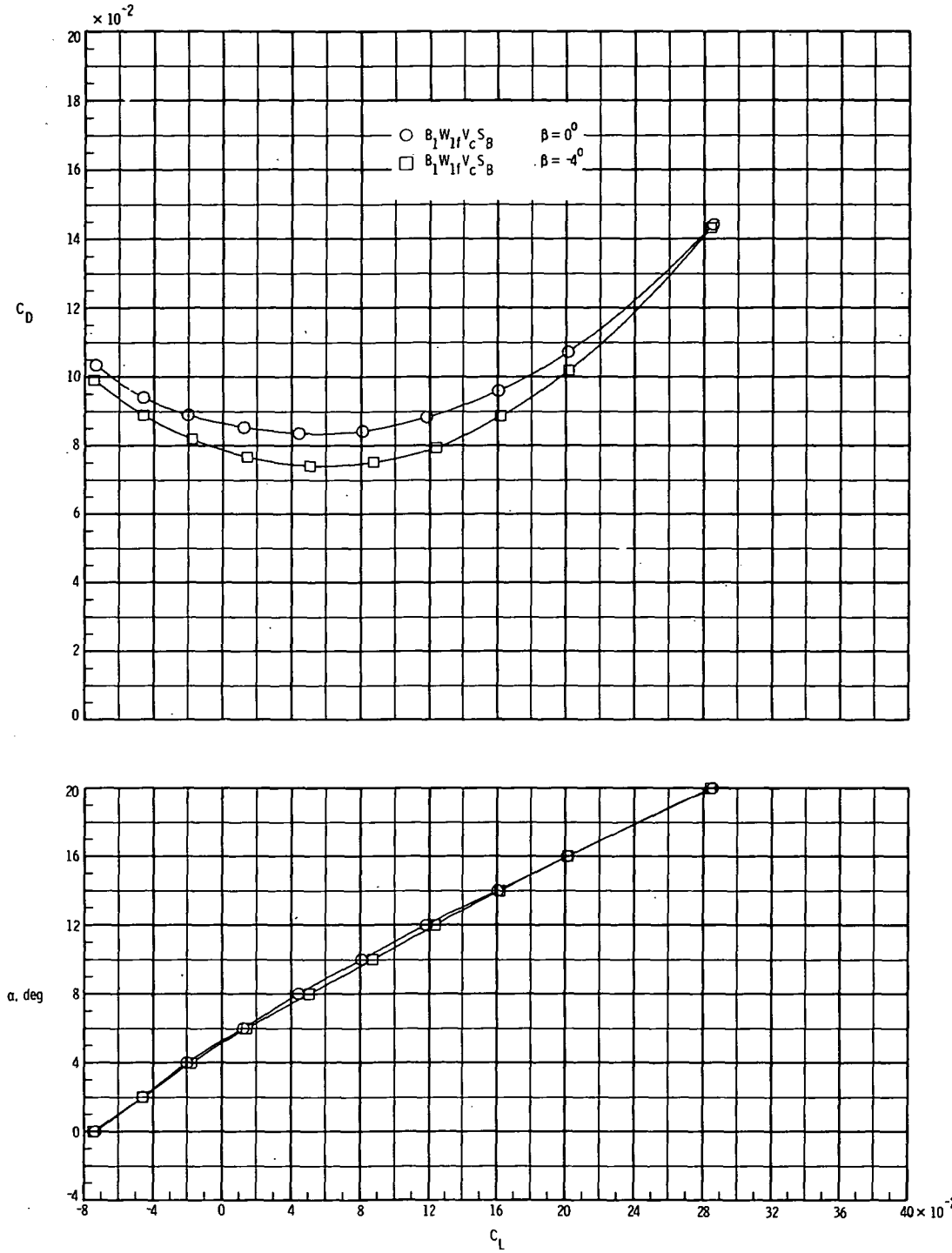


(b) Drag and lift.

Figure 21.- Concluded.

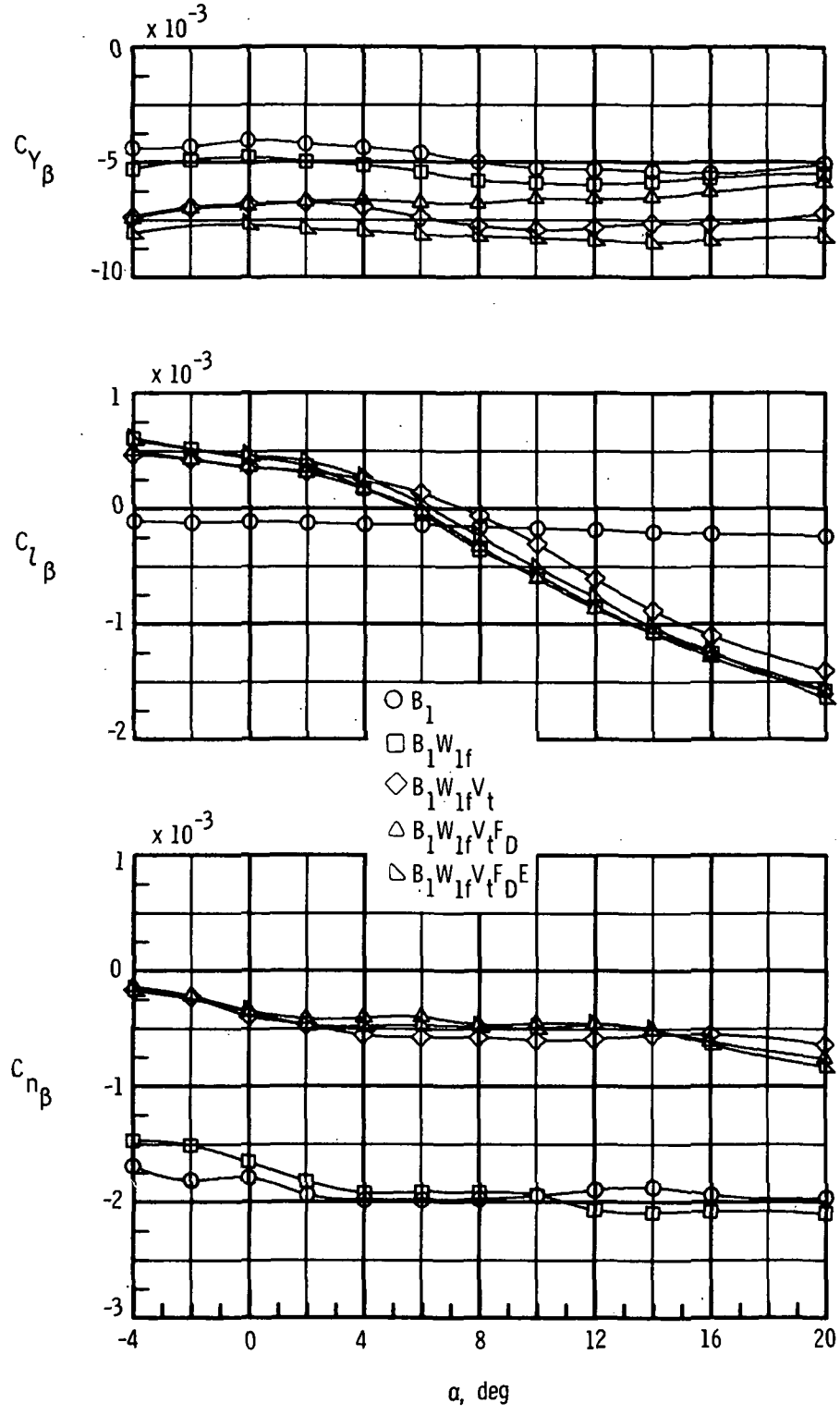


Figure 22.- Effect of component buildup on lateral-directional characteristics with body $B_1$.

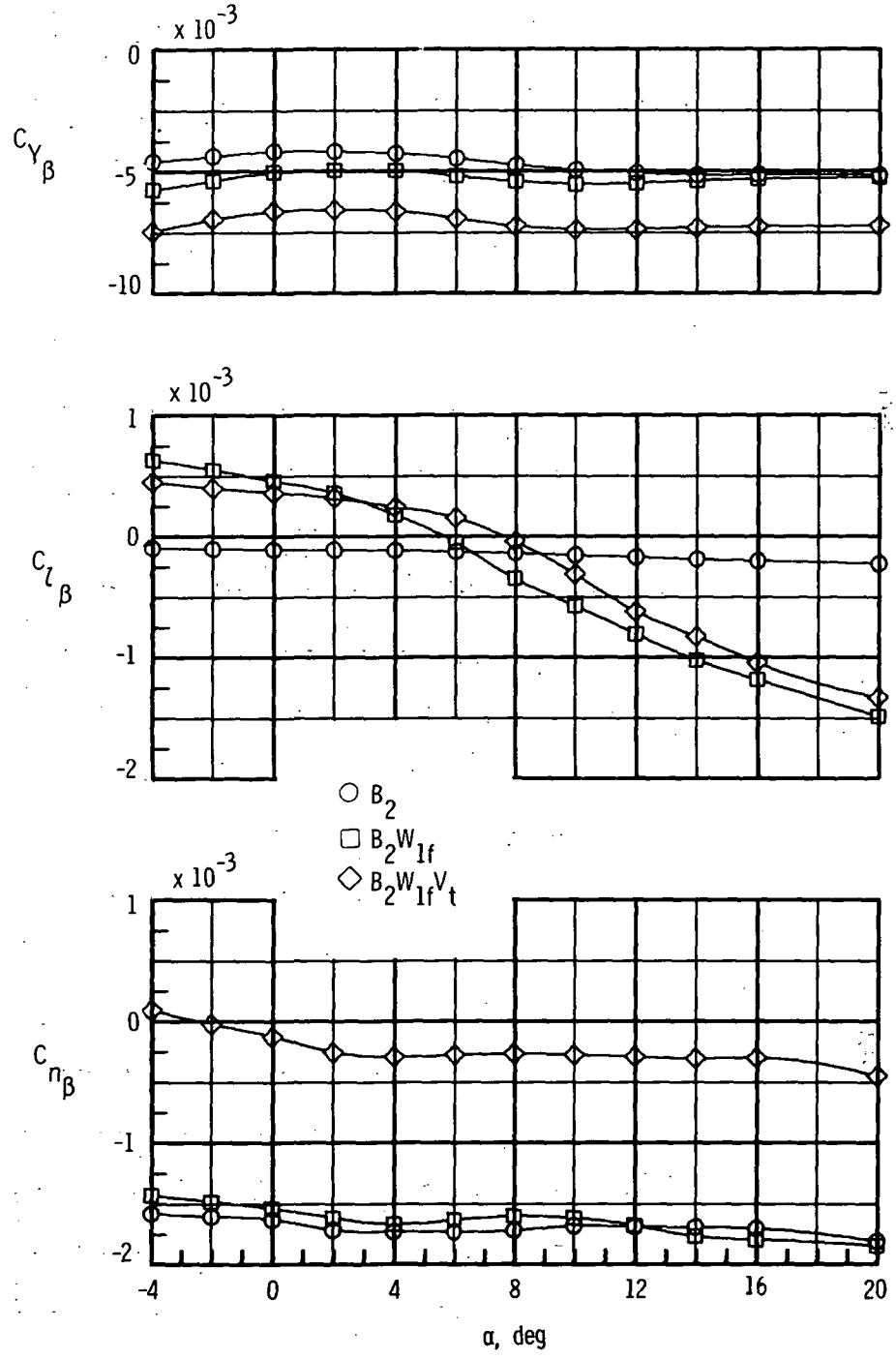


Figure 23.- Effect of component buildup on lateral-directional characteristics with body $B_2$.

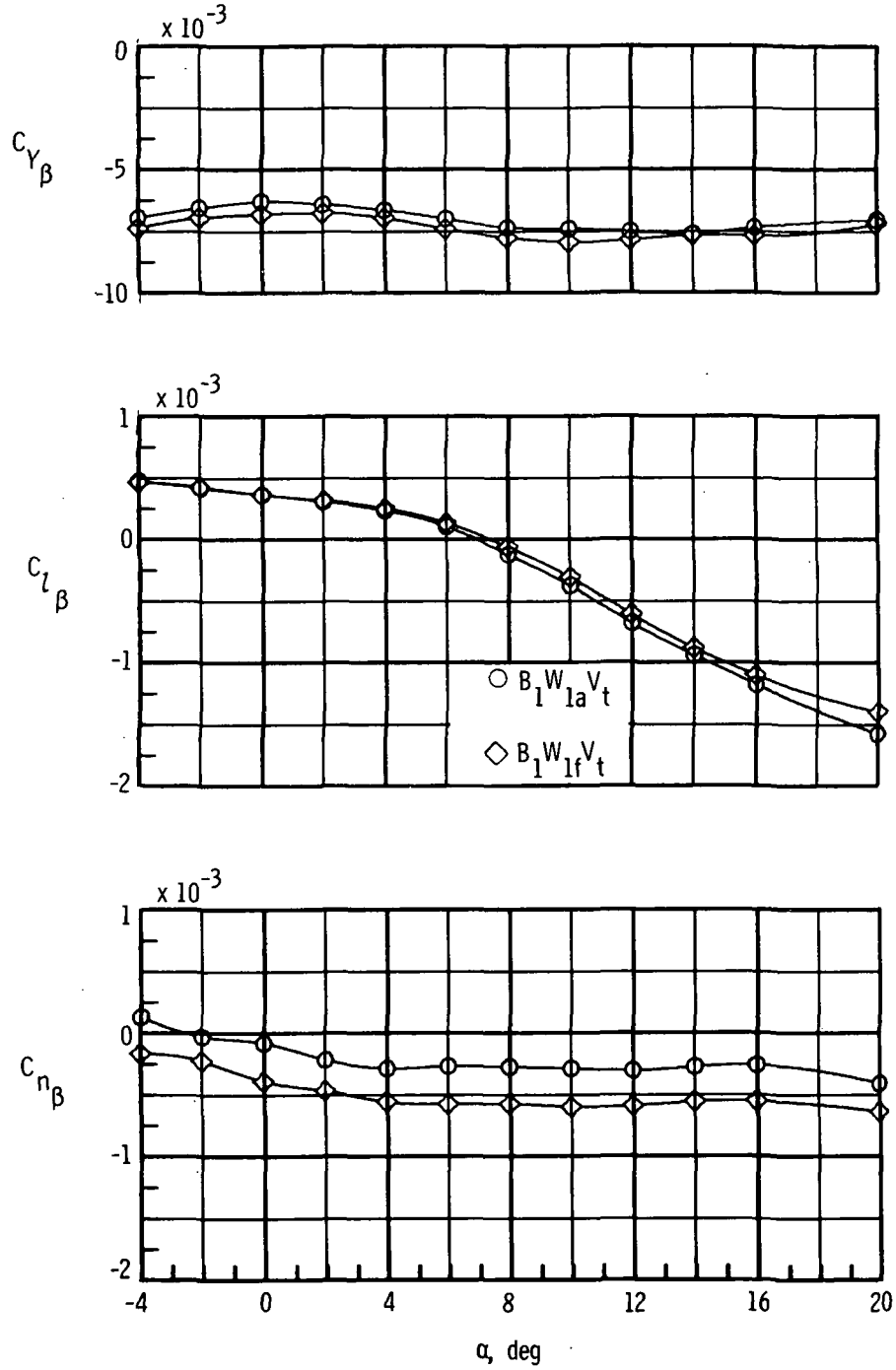


Figure 24.- Effect of wing location on lateral-directional characteristics.

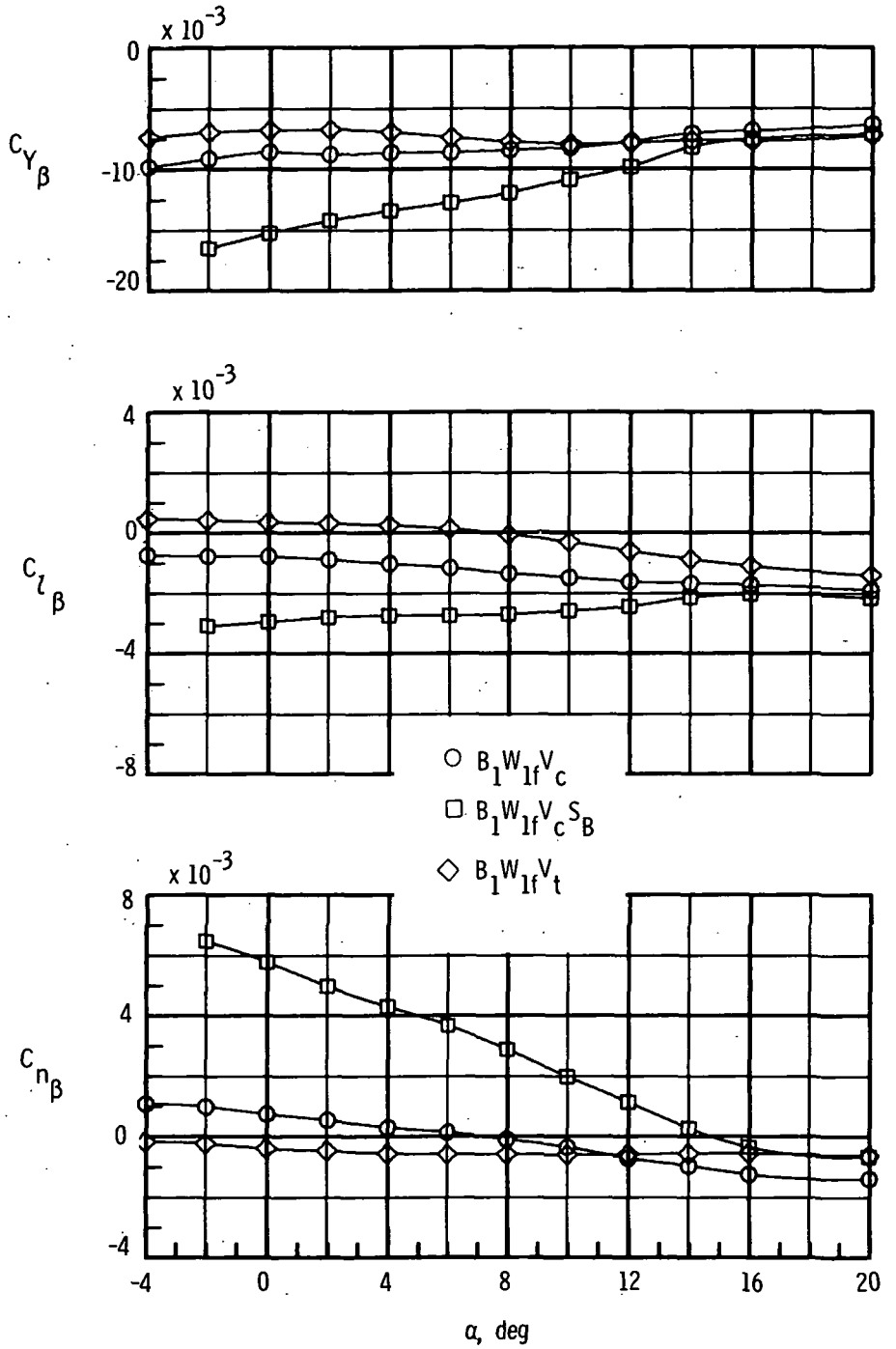


Figure 25.- Comparison of the effect of center vertical tail, wing tip fins, and 20° speed brakes on lateral-directional characteristics.

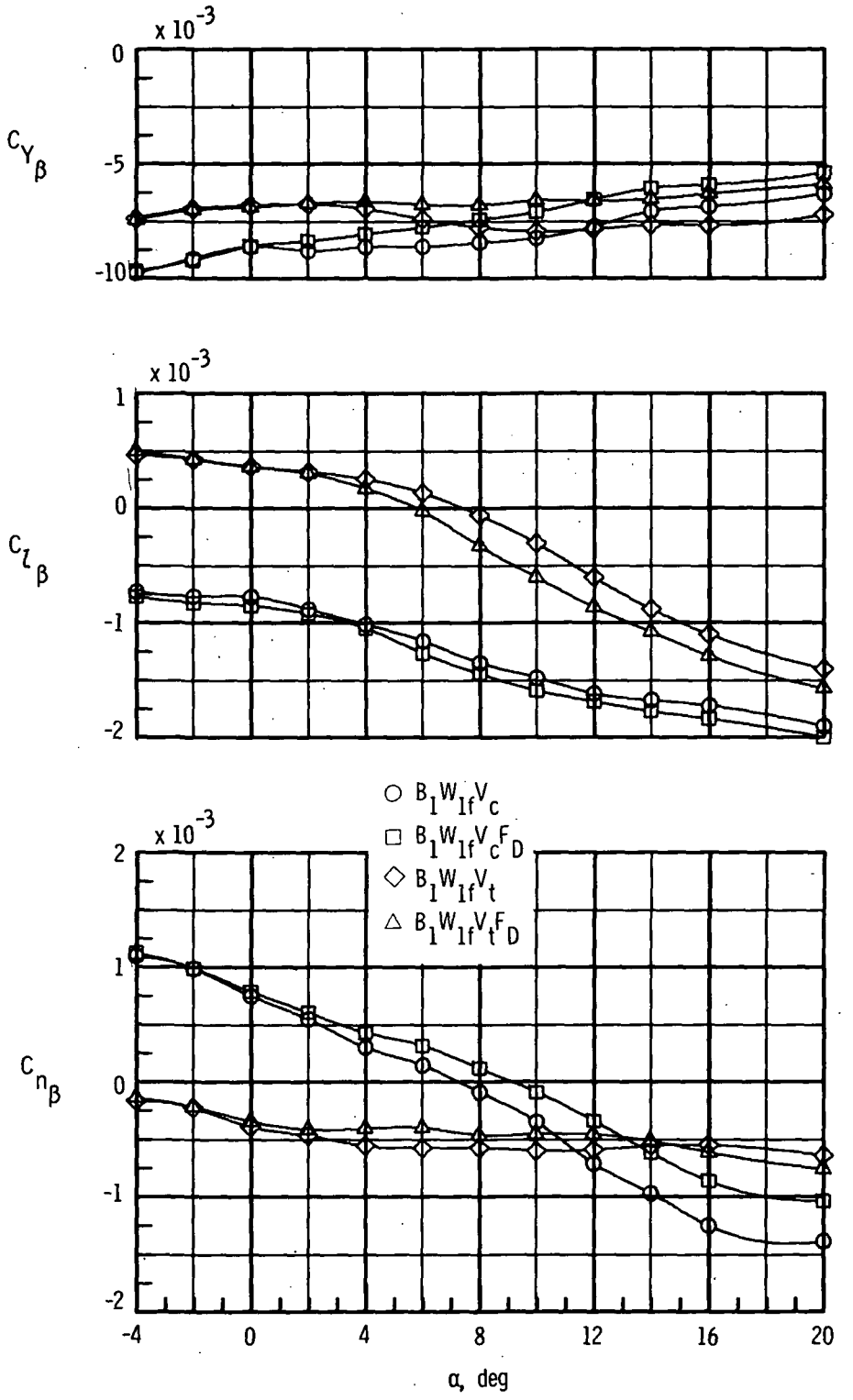


Figure 26.- Effect of forward delta wing on lateral-directional characteristics.

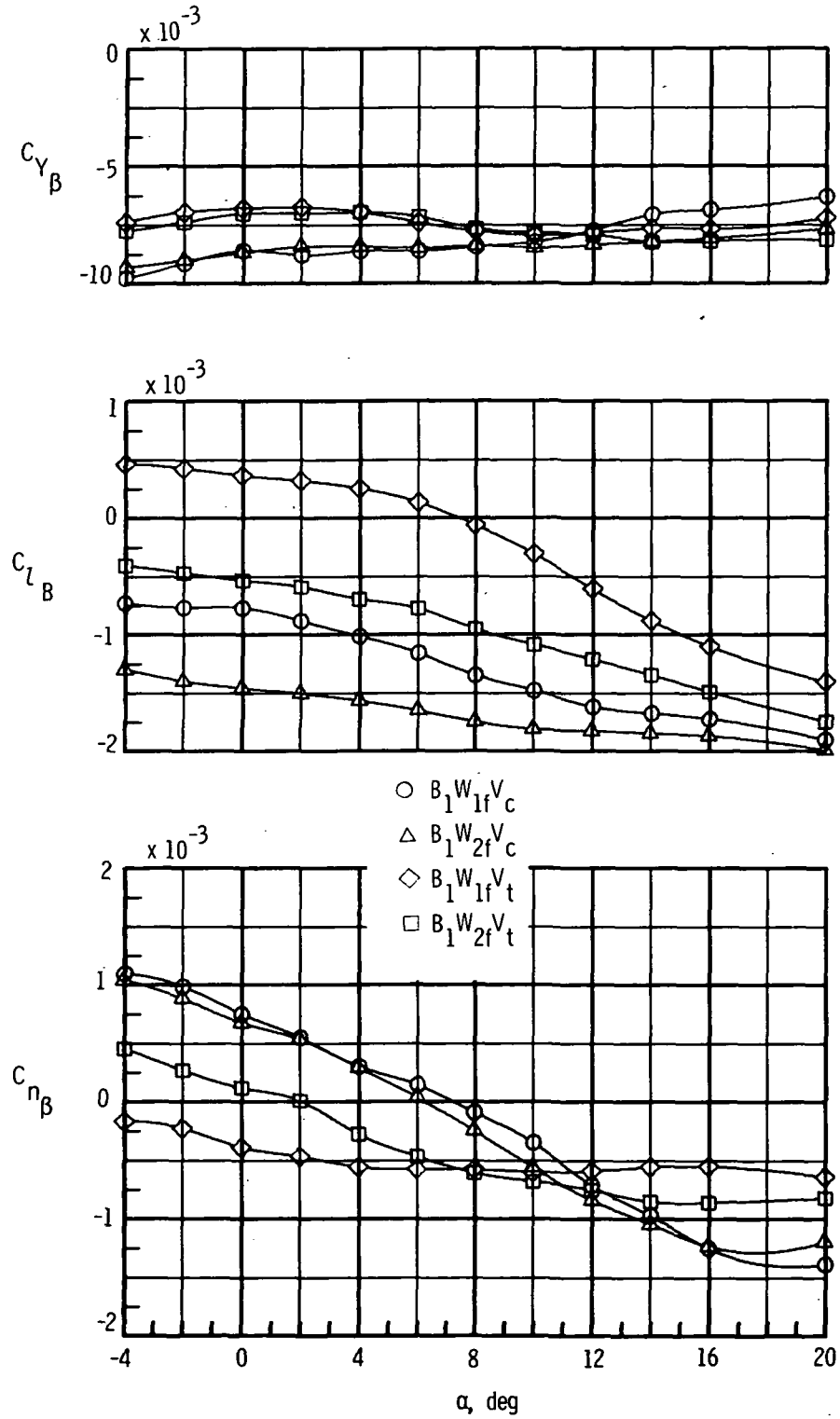


Figure 27.- Effect of wing camber on lateral-directional characteristics; $\delta = 0^o$.

NATIONAL AERONAUTICS AND SPACE ADMINISTRATION
WASHINGTON, D.C. 20546

OFFICIAL BUSINESS
PENALTY FOR PRIVATE USE $300

SPECIAL FOURTH-CLASS RATE BOOK

POSTAGE AND FEES PAID
NATIONAL AERONAUTICS AND SPACE ADMINISTRATION
451

U.S.MAIL

POSTMASTER: If Undeliverable (Section 158 Postal Manual) Do Not Return

*"The aeronautical and space activities of the United States shall be conducted so as to contribute . . . to the expansion of human knowledge of phenomena in the atmosphere and space. The Administration shall provide for the widest practicable and appropriate dissemination of information concerning its activities and the results thereof."*

—NATIONAL AERONAUTICS AND SPACE ACT OF 1958

# NASA SCIENTIFIC AND TECHNICAL PUBLICATIONS

TECHNICAL REPORTS: Scientific and technical information considered important, complete, and a lasting contribution to existing knowledge.

TECHNICAL NOTES: Information less broad in scope but nevertheless of importance as a contribution to existing knowledge.

TECHNICAL MEMORANDUMS: Information receiving limited distribution because of preliminary data, security classification, or other reasons. Also includes conference proceedings with either limited or unlimited distribution.

CONTRACTOR REPORTS: Scientific and technical information generated under a NASA contract or grant and considered an important contribution to existing knowledge.

TECHNICAL TRANSLATIONS: Information published in a foreign language considered to merit NASA distribution in English.

SPECIAL PUBLICATIONS: Information derived from or of value to NASA activities. Publications include final reports of major projects, monographs, data compilations, handbooks, sourcebooks, and special bibliographies.

TECHNOLOGY UTILIZATION PUBLICATIONS: Information on technology used by NASA that may be of particular interest in commercial and other non-aerospace applications. Publications include Tech Briefs, Technology Utilization Reports and Technology Surveys.

***Details on the availability of these publications may be obtained from:***

**SCIENTIFIC AND TECHNICAL INFORMATION OFFICE**

**NATIONAL AERONAUTICS AND SPACE ADMINISTRATION**

**Washington, D.C. 20546**